JCI The Journal of Clinical Investigation

Inflammatory cytokine–regulated tRNA-derived fragment *tRF-21* suppresses pancreatic ductal adenocarcinoma progression

Ling Pan, … , Dongxin Lin, Jian Zheng

J Clin Invest. 2021;131(22):e148130. https://doi.org/10.1172/JCI148130.

Research Article | Oncology | Therapeutics

Graphical abstract

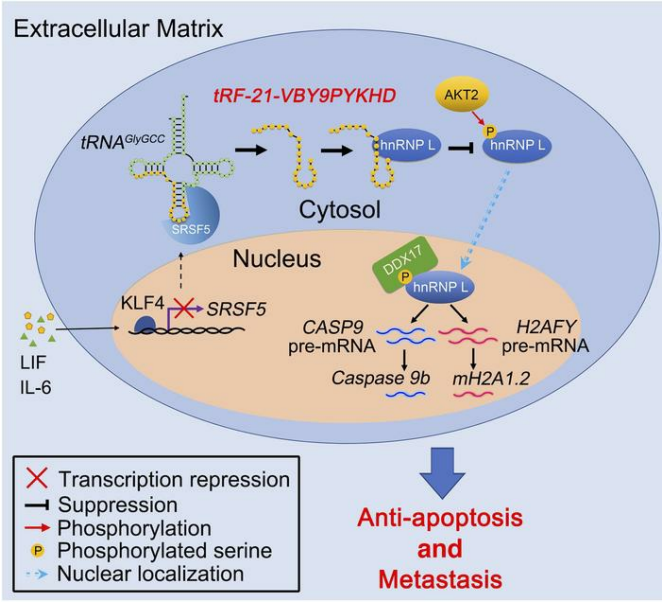

Find the latest version:

https://jci.me/148130/pdf

Inflammatory cytokine–regulated tRNA-derived fragment *tRF-21* suppresses pancreatic ductal adenocarcinoma progression

Ling Pan,[1] Xudong Huang,[1] Ze-Xian Liu,[1] Ying Ye,[1] Rui Li,[1] Jialiang Zhang,[1] Guandi Wu,[1] Ruihong Bai,[1] Lisha Zhuang,[1] Lusheng Wei,[2] Mei Li,[3] Yanfen Zheng,[1] Jiachun Su,[1] Junge Deng,[1] Shuang Deng,[1] Lingxing Zeng,[1] Shaoping Zhang,[1] Chen Wu,[4] Xu Che,[5] Chengfeng Wang,[5] Rufu Chen,[6] Dongxin Lin,[1,4,7] and Jian Zheng[1,7]

[1]Sun Yat-sen University Cancer Center, State Key Laboratory of Oncology in South China and Collaborative Innovation Center for Cancer Medicine, Guangzhou, China. [2]Department of Pancreaticobiliary Surgery, Sun Yat-sen Memorial Hospital, Sun Yat-sen University, Guangzhou, China. [3]Department of Pathology, Sun Yat-sen University Cancer Center, Guangzhou, China. [4]Department of Etiology and Carcinogenesis, National Cancer Center/National Clinical Research Center/Cancer Hospital, Chinese Academy of Medical Sciences and Peking Union Medical College, Beijing, China. [5]Department of Abdominal Surgery, National Cancer Center/National Clinical Research Center/Cancer Hospital, Chinese Academy of Medical Sciences and Peking Union Medical College, Beijing, China. [6]Guangdong Provincial People's Hospital and Guangdong Academy of Medical Sciences, Guangzhou, China. [7]Jiangsu Key Laboratory of Cancer Biomarkers, Prevention and Treatment, Collaborative Innovation Center for Cancer Medicine, Nanjing Medical University, Nanjing, China.

The tumorigenic mechanism for pancreatic ductal adenocarcinoma (PDAC) is not clear, although chronic inflammation is implicated. Here, we identified an inflammatory cytokine–regulated transfer RNA–derived (tRNA-derived) fragment, *tRF-21-VBY9PYKHD* (*tRF-21*), as a tumor suppressor in PDAC progression. We found that the biogenesis of *tRF-21* could be inhibited by leukemia inhibitory factor and IL-6 via the splicing factor SRSF5. Reduced *tRF-21* promoted AKT2/1-mediated heterogeneous nuclear ribonucleoprotein L (hnRNP L) phosphorylation, enhancing hnRNP L to interact with dead-box helicase 17 (DDX17) to form an alternative splicing complex. The provoked hnRNP L-DDX17 activity preferentially spliced *Caspase 9* and *mH2A1* pre-mRNAs to form *Caspase 9b* and *mH2A1.2*, promoting PDAC cell malignant phenotypes. The *tRF-21* levels were significantly lower in PDACs than in normal tissues, and patients with low *tRF-21* levels had a poor prognosis. Treatment of mouse PDAC xenografts or patient-derived xenografts (PDXs) with *tRF-21* mimics repressed tumor growth and metastasis. These results demonstrate that *tRF-21* has a tumor-suppressive effect and is a potential therapeutic agent for PDAC.

Introduction

Pancreatic ductal adenocarcinoma (PDAC) is the most lethal malignancy, with a 5-year survival rate of less than 9% (1, 2). Most PDAC tumors are already in an advanced stage when they are diagnosed and are thus beyond the time window for effective treatment. Extensive tolerance to chemoradiotherapy makes PDAC clinical outcomes extremely poor. Metastasis occurs quickly by invasion of the adjacent organs or through lymphatic or vascular tracts and is the major cause of death. Hence, it is crucial to uncover the molecular mechanisms underlying PDAC development and progression in order to identify new targets for treatment of the disease.

It is well known that the tumor microenvironment (TME) plays an essential role in tumor progression, including invasiveness and metastasis. A large number of stromal components, including various types of signaling molecules such as tumor-promoting cytokines released by inflammatory cells, are present in the PDAC TME (3). Long-term stimulation of inflammatory cytokines causes chronic pancreatitis, which may consequently induce PDAC and accelerate PDAC progression (4, 5). For example, chronic pancreatitis may augment the effect of mutated KRAS on IL-17 receptor induction and IL-17–producing immune cell infiltration (6). The cytokines TNF-α, IL-6, IL-1α, leukemia inhibitory factor (LIF), and IL-10 have been reported to contribute to pancreatic cancer progression (7–14). However, how these cytokines promote PDAC progression and malignant phenotypes is largely unknown.

In recent years, noncoding RNAs (ncRNAs) have attracted great attention in cancer research because of their vital biological functions. Transfer RNA–derived small RNAs (tsRNAs) belong to a family of short ncRNAs presented in most organisms. tsRNAs are generated constitutively and in the context of stresses by several enzymes or proteins such as Dicer (15), angiogenin (16) and RNase Z (17) that are further subdivided into transfer RNA (tRNA) halves (tRHs; >30 nt) and tRNA-derived fragment (tRFs; <30 nt). Multiple classes of tRFs have been identified that are generated by enzymatic cleavage at different sites in mature tRNAs, including 5′-tRFs, 3′-tRFs, and i-tRFs (18). Of these, iTRFs, which originate from the internal body of mature tRNAs, have an atypical length that extends from the D-loop to the T-loop of mature tRNAs and straddle the anticodon. Some tRFs function similarly to miRNAs

Authorship note: LP, XH, ZL, and YY contributed equally to this work.
Conflict of interest: The authors have declared that no conflict of interest exists.

Submitted: January 27, 2021; **Accepted:** September 28, 2021;
Published: November 15, 2021.
Reference information: *J Clin Invest*. 2021;131(22):e148130.
https://doi.org/10.1172/JCI148130.

(19, 20) and are involved in cancer development and progression. For example, *CU1276*, a 3′-tRF derived from $tRNA^{GlyGCC}$, has been shown to bind to Argonaute protein, thereby repressing replication protein A1 expression and inhibiting cell proliferation (21). A tRF generated from $tRNA^{Leu}$ can suppress stem cell–like cells and metastasis in colorectal cancer by targeting the Notch ligand JAG2 (22). It has been documented that tRFs derived under hypoxic conditions in breast cancer cells from $tRNA^{Glu}$, $tRNA^{Asp}$, $tRNA^{Gly}$, and $tRNA^{Tyr}$ may engage oncogenic RNA-binding protein YBX1 and displace YBX1 from the 3′-UTRs of multiple oncogenic transcripts, leading to its degradation and thus suppressing cancer metastasis (23). Moreover, tRFs may alter mRNA conformation influencing the translation process. For instance, the tRF *LeuCAG3′tsRNA* can bind RPS28 mRNA, enhancing the mRNA translation by unfolding its secondary structure (24). However, whether the biogenesis of tRFs can be regulated by certain cytokines and, if yes, what and how they play in PDAC development and progression remain to be elucidated.

In the present study, with the hypothesis of interaction between inflammatory cytokines and tRFs, we have identified a serine- and arginine-rich splicing factor 5–mediated (SRSF5-mediated) LIF and an IL-6–regulated i-tRF, *tRF-21-VBY9PYKHD* (*tRF-21*), based on deep mining of The Cancer Genome Atlas (TCGA; https://tcga-data.nci.nih.gov/tcga/) pancreatic adenocarcinoma (PAAD) sRNA-Seq data. We demonstrated that *tRF-21* bound to and prevented heterogeneous nuclear ribonucleoprotein L (hnRNP L) from phosphorylation by AKT2/1 and thus restrained the formation of hnRNP L-DEAD-box helicase 17 (DDX17), an RNA splicing complex. The altered hnRNP L-DDX17 activity affected *Caspase 9* and *mH2A1* pre-mRNA splicing, which is linked to PDAC cell malignant phenotypes. We found that patients with low *tRF-21* levels in PDAC tumors had shorter survival than did those with high tumor levels of *tRF-21*. We also show that *tRF-21* is a potential therapeutic agent for PDAC.

Results

tRF-21 is associated with PDAC prognosis. We started with TCGA PAAD database to search for tRFs associated with survival in 177 patients, and univariate Cox regression analysis showed that among 368 tRFs in the short RNA data, 23 were significantly associated with patient survival times (Figure 1A). We selected the top 10 candidates from the 23 associated tRFs (Supplemental Table 1; supplemental material available online with this article; https://doi.org/10.1172/JCI148130DS1) for validation in our patient sample (cohort 1) and found that only the levels of *tRF-21* in PDAC determined by quantitative reverse transcription PCR (qRT-PCR) were associated with survival time (Figure 1B), with an adjusted HR of 0.47 for death for high levels (95% CI, 0.32–0.69). Kaplan-Meier estimates showed that patients with PDAC who had high *tRF-21* levels had significantly longer survival than did PDAC patients with low *tRF-21* levels in cohort 1 (n = 158; Figure 1C, left panel), cohort 2 (n = 69; Figure 1C, middle panel), or a pooled sample (n = 227; Figure 1C, right panel). We further compared *tRF-21* levels according to tumor or normal status and according to different tumor stages. The results showed that *tRF-21* levels were significantly lower in PDAC tumors than in adjacent normal tissues (Figure 1D) and significantly lower in advanced-stage tumors (stages III/IV) than in early-stage tumors (stages I/II) in both cohorts 1 and 2 (Figure 1E). We also consulted TCGA database, and the results showed that the median level of *tRF-21* was nonsignificantly lower in PAAD compared with levels in adjacent normal pancreatic tissue (P = 0.0861; Supplemental Figure 1A). However, this comparison was based on only 3 adjacent normal samples, which had very limited statistical power. Together, these results indicate that *tRF-21* is involved in PDAC progression.

We then wanted to confirm the identity of *tRF-21*, which has been reported to derive from mature $tRNA^{GlyGCC}$ (25). We first examined the levels of *tRF-21* in 7 commonly used PDAC cell lines (Supplemental Figure 1B). Sanger sequencing of the PCR product amplified using our stem-loop primers showed exactly the same sequence as that of *tRF-21* (Supplemental Figure 1C). Northern blot analysis confirmed the existence of *tRF-21* in PDAC cells (Supplemental Figure 1D). Cell fractionation and FISH analyses showed that *tRF-21* was predominantly present in the cytoplasm (80%–90%; Supplemental Figures 1, E and F). Because Capan-2 and SW1990 cell lines had moderate *tRF-21* levels (Supplemental Figure 1B), they were suitable for experimental operation and were thus chosen for further analysis throughout this study.

tRF-21 acts as a tumor suppressor in PDAC. We next examined the effects of *tRF-21* on PDAC cell phenotypes by increasing or decreasing its level in cells (Supplemental Figure 2A). We found that, although changing *tRF-21* levels in PDAC cells did not alter the cellular mature $tRNA^{GlyGCC}$ levels (Supplemental Figure 2, B and C), increasing *tRF-21* significantly repressed cell growth ability, while decreasing *tRF-21* had the opposite effect (Figure 2, A and B, and Supplemental Figure 2D), and this was likely due to the inhibitory effect of *tRF-21* on cell apoptosis (Figure 2C and Supplemental Figure 2E). We also found that increasing *tRF-21* levels significantly reduced the invasive ability of PDAC cells, whereas decreasing *tRF-21* levels significantly enhanced this ability (Figure 2D and Supplemental Figure 2F). These effects were further verified in vivo in mouse xenograft models. Subcutaneous xenografts derived from PDAC cells with high *tRF-21* levels had significantly reduced growth rates, but tumors derived from PDAC cells with low *tRF-21* levels had significantly increased growth rates compared with controls (Figures 2E and Supplemental Figure 2G). Pancreatic xenografts derived from PDAC cells with high *tRF-21* levels had significantly reduced growth rates, less distant metastases, and longer survival, while tumors derived from cells with low *tRF-21* levels had opposite phenotypes compared with controls (Figure 2, F–H, Supplemental Figure 2H, and Supplemental Figure 3, A–C). Taken together, these results indicate that *tRF-21* acts as a tumor suppressor that inhibits PDAC malignant phenotypes.

tRF-21 prevents hnRNP L from phosphorylation by AKT2. To seek the functional mechanism underlying the inhibitory effects of *tRF-21* on PDAC, we first performed RNA-pulldown assays using biotinylated *tRF-21* or its antisense oligonucleotide (oligo) with PDAC cell lysates, followed by mass spectrometric analysis. The results indicated that at least 38 proteins might specifically interact with *tRF-21*, but not its antisense RNA. We then selected the top 7 proteins ranked by abundance for further validation (Figure 3A and Supplemental Table 2) and found that, among them, only hnRNP L, a key player in alternative mRNA splic-

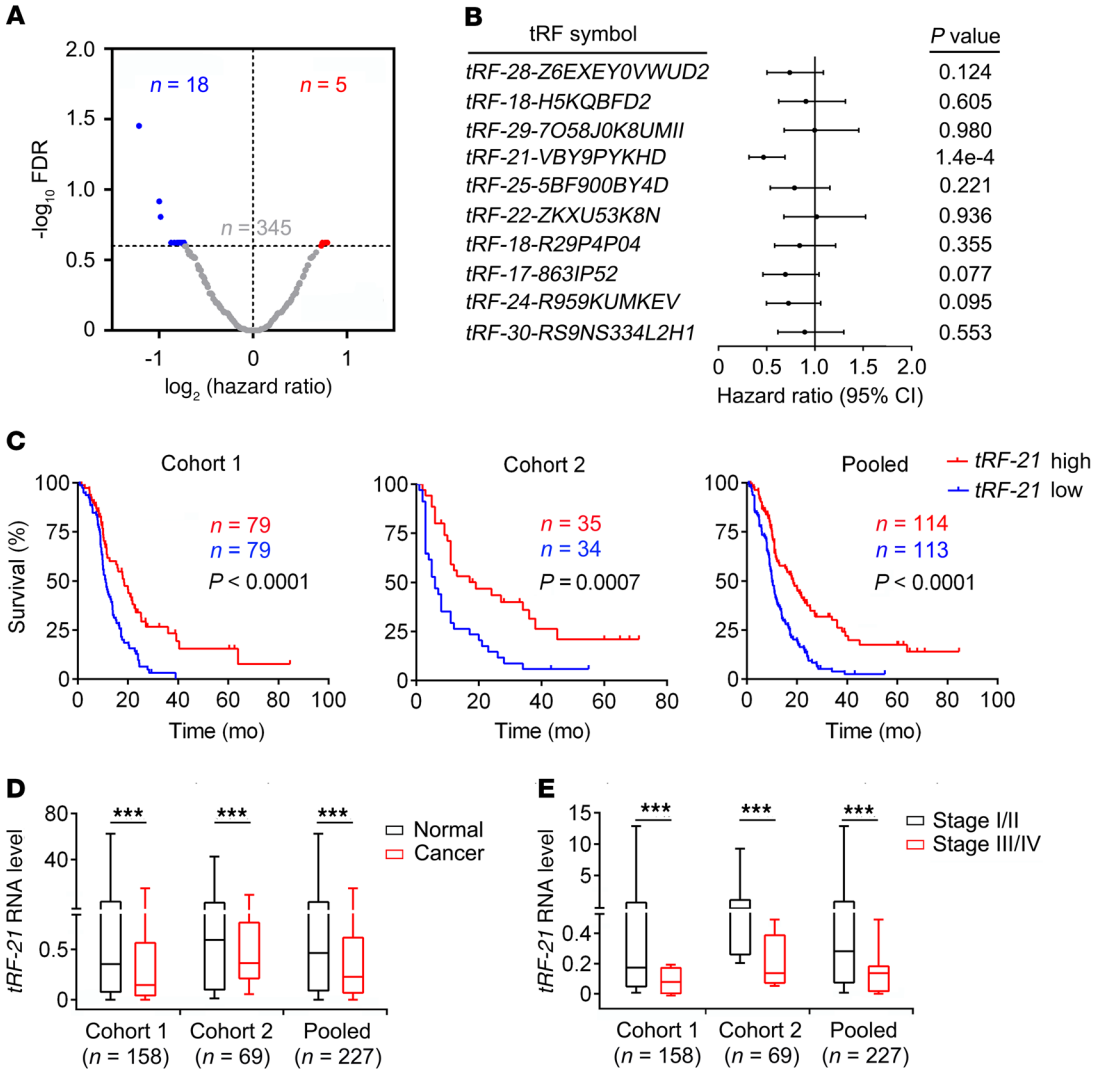

Figure 1. *tRF-21* is associated with survival time in patients with PDAC. (**A**) Volcano plot of tRFs associated with survival time in TCGA PAAD patients. Red and blue dots represent a FDR below 0.25, whereas gray dots represent a FDR of 0.25 or higher. (**B**) Associations of the expression levels of 10 tRFs with survival time for patients in cohort 1, showing a significant association only for *tRF-21*. (**C**) Kaplan-Meier estimates of patients' survival time in cohort 1, cohort 2, and a combined sample according to *tRF-21* levels in PDAC. The median survival times for patients with high *tRF-21* levels (≥ the median) in cohort 1, cohort 2, and a combined sample were 18.4, 19.0, and 18.4 months, significantly longer than 11.2, 6.0, and 10.1 months for patients with low *tRF-21* levels (< the median), with the HRs (95% CI) for death of 0.47 (95% CI, 0.32–0.69), 0.49 (95% CI, 0.26–0.93), and 0.48 (95% CI, 0.35–0.65), respectively, for patients with high *tRF-21* levels. *P* values were determined by log-rank test. (**D** and **E**) *tRF-21* levels were significantly lower in PDAC than in paired normal tissues (**D**) and in stage III/IV tumors than in stage I/II tumors (**E**). Data are shown in box plots; the lines in the middle of the box indicate the median, and the upper and lower lines indicate the 25th and 75th percentiles. ***$P < 0.001$, by Wilcoxon rank-sum test (**D** and **E**). $n = 136$ stage I/II tumors and $n = 22$ stage III/IV tumors for cohort 1; and $n = 47$ stage I/II tumors and $n = 22$ stage III/IV tumors for cohort 2.

ing (26), interacted with *tRF-21*, as determined by Western blot analysis of the RNA-pulldown product using either the antisense oligo or the nontargeting oligo (Figure 3B). Similarly, RNA immunoprecipitation (RIP) assays with an antibody against hnRNP L also confirmed the specific interaction of *tRF-21* with hnRNP L in PDAC cells (Figure 3C). Because both mRNA and protein levels of hnRNP L were not significantly changed when *tRF-21* levels were altered in cells (Figure 3D), we turned to examining whether *tRF-21* interaction may affect hnRNP L posttranslational modification. We first performed protein domain mapping assays with FLAG-tagged and truncated hnRNP L and *tRF-21* and found that the Gly-rich domain in hnRNP L protein was required for their interaction (Figure 3E). A previous report (27) suggested that Tyr47, Tyr48, and Ser52 in the hnRNP L Gly-rich domain can be phosphorylated, and phosphorylation at Ser52 is required for hnRNP L activation (Figure 3F). We then examined whether *tRF-21* can affect Ser52 phosphorylation by performing RNA-pulldown assays with cellular lysates of PDAC cells transfected with FLAG-tagged hnRNPL or hnRNP L constructs with mutation at the Tyr47, Tyr48, or Ser52 site. Interestingly, the results showed that *tRF-21* was unable to bind the Ser52Ala mutant hnRNP L, although the Tyr47 and Tyr48 mutations had no such effect (Figure 3G). RIP assays also confirmed the specific binding of *tRF-21* with Ser52–hnRNP L (Figure 3H). The computational

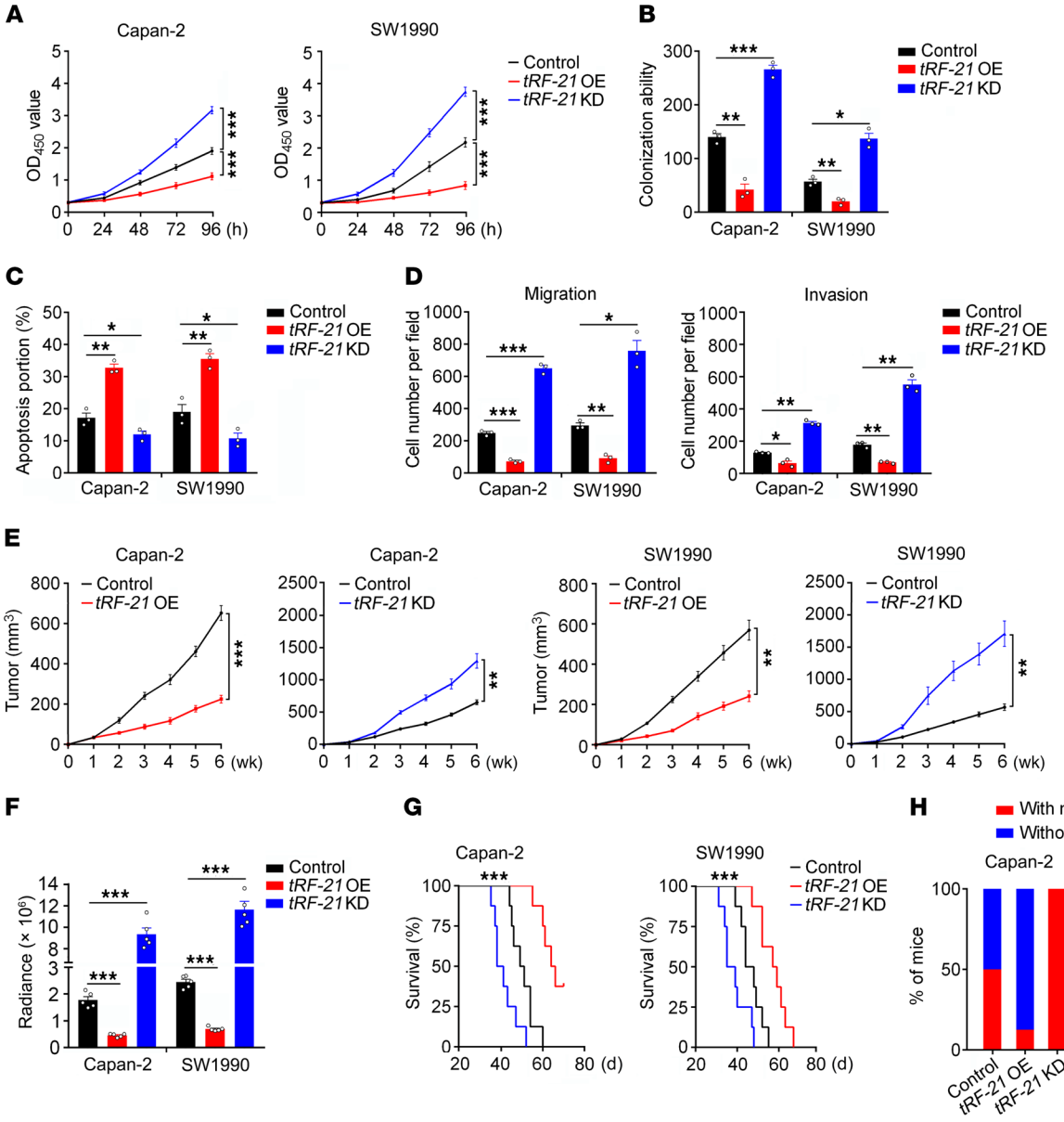

Figure 2. *tRF-21* suppresses the malignant phenotypes of PDAC cells in vitro and in vivo. (**A**–**D**) Effects of *tRF-21* overexpression (OE) or silencing (KD) on PDAC cell proliferation (**A**), colony formation (**B**), apoptosis (**C**), and migration and invasion (**D**). Data indicate the mean ± SEM and represent at least 3 independent experiments. (**E**) Effect of *tRF-21* expression changes on PDAC xenograft growth in mice. Shown are the growth curves of the xenografts. Data indicate the mean ± SEM ($n = 5$). (**F**) Fluorescence intensity data showing the effect of *tRF-21* expression changes on tumor burdens in mice with orthotopically transplanted PDAC ($n = 5$). Data indicate the mean ± SEM. (**G**) Effect of *tRF-21* expression changes on survival times of mice with orthotopically transplanted PDAC ($n = 8$). (**H**) Tumor metastasis in mice from each group. Organs with metastatic tumors are shown in Supplemental Figure 3. $^*P < 0.05$, $^{**}P < 0.01$, and $^{***}P < 0.001$, by 1-way ANOVA with Dunnett's T3 multiple-comparison test (**A**–**F**) and log-rank test (**G**).

model structure analysis also indicated that Ser52 is a critical residue of hnRNP L for *tRF-21* binding (Figure 3I). Last, we performed Western blotting with an antibody against phosphorylated hnRNP L at Ser52 (p–Ser52–hnRNP L) to detect whether hnRNP L phosphorylation changes in cells with forced alteration of *tRF-21* levels, and the findings clearly showed that increasing or decreasing *tRF-21* levels resulted in substantial repression or promotion of the phosphorylation (Figure 4A). Since AKT2 has been shown to phosphorylate hnRNP L at Ser52 in lung cancer cells (28), we established 293T and PDAC cells overexpressing constitutively active AKT2 (Myr HA AKT2) (29) to verify this finding and to examine the effect of *tRF-21*. As a result, in these cells, p–Ser52–hnRNP L levels were substantially increased, but the phosphorylation of mutant Ala52-hnRNP L (p–Ala52–hnRNP L) was negligible. Furthermore, treatment of cells with phosphatase substantially abolished p–Ser52–hnRNP L levels (Figure 4, B and C). We also performed in vitro assays with recombinant human AKT2 and found that *tRF-21* had the ability to prevent hnRNP L from phosphorylation but that its antisense RNA had no such effect (Figure 4D). Further assays showed that overexpression of *tRF-21* in cells markedly reduced Ser52–hnRNP L phosphorylation, and this phenomenon could not be recovered, even

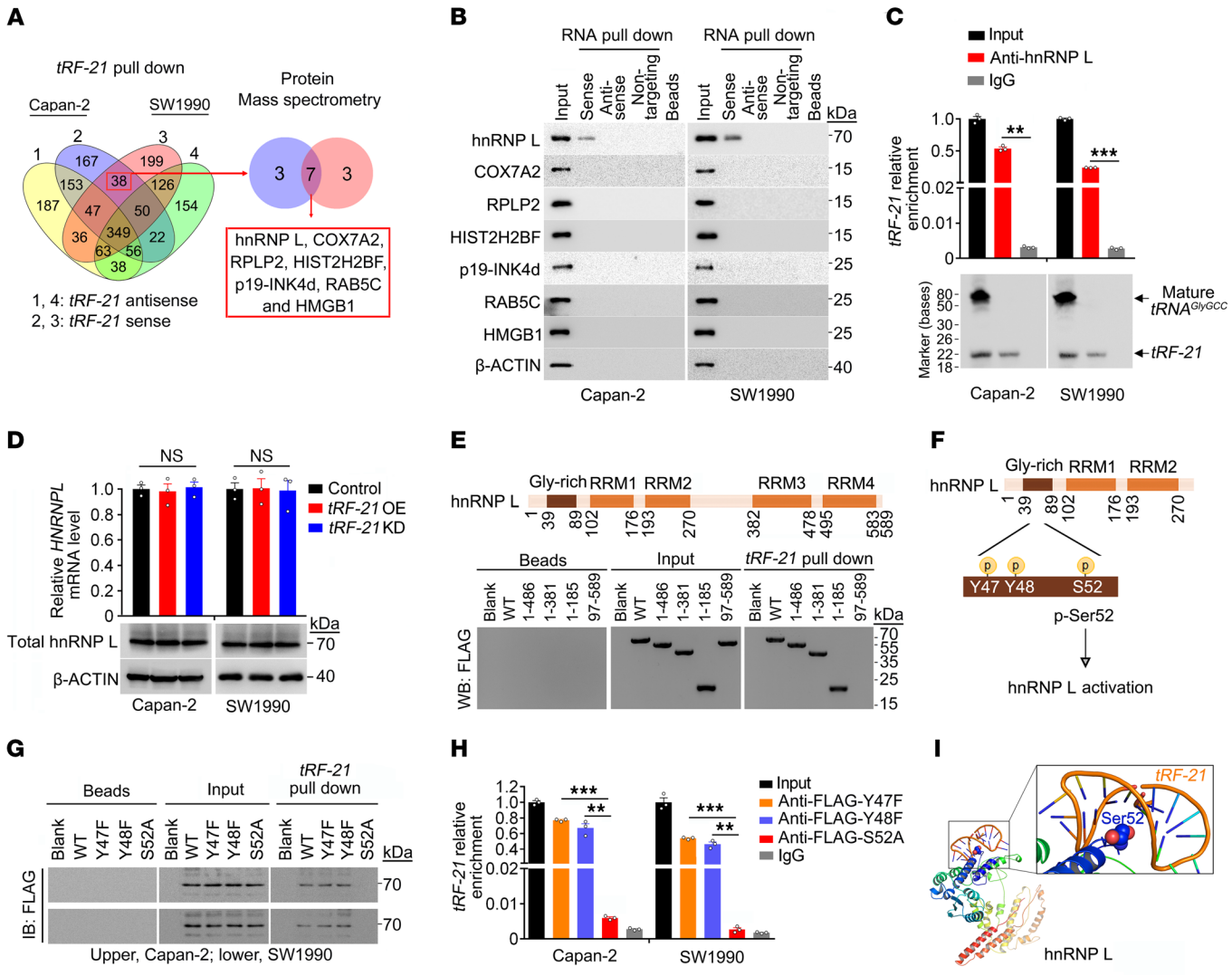

Figure 3. *tRF-21* interacts with hnRNP L at Ser52. (**A**) Schematic of the RNA-pulldown assay followed by liquid chromatography–mass spectrometry (LC-MS) using a *tRF-21* sense or antisense probe for the identification of proteins that specifically bind *tRF-21*. (**B**) Western blot analysis of products from RNA-pulldown assays using *tRF-21*, *tRF-21* antisense, or a nontargeting oligo suggested 7 potential *tRF-21*–binding proteins. (**C**) Association of hnRNP L with *tRF-21* in PDAC cells determined by RIP assays followed by qRT-PCR or Northern blotting. qRT-PCR data represent enrichment (mean ± SEM) relative to input from 3 independent experiments. IgG was used as a negative control. (**D**) *tRF-21* overexpression or silencing did not affect *HNRNPL* mRNA or protein levels. qRT-PCR data indicate the mean ± SEM of 3 independent experiments. (**E**) Truncation mapping of the *tRF-21*–hnRNP L binding domain. Schematic diagram shows the FLAG-tagged hnRNP L protein domain structure. Western blot (WB) shows FLAG-tagged full-length (WT) hnRNP L and its truncated forms pulled down by *tRF-21*. (**F**) Schematic of phosphorylation sites in the Gly-rich domain; Ser52 is responsible for the activation of hnRNP L. (**G**) Immunoblot (IB) shows FLAG-tagged full-length hnRNP L (WT) and its mutated forms (Y47F, Y48F, and S52A) retrieved by *tRF-21*. (**H**) RIP assays with an antibody against FLAG showed that FLAG-Y47F and FLAG-Y48F, but not FLAG-S52A, interacted with *tRF-21*. Data represent enrichment (mean ± SEM) relative to input from 3 independent experiments. IgG was used as a negative control. (**I**) Predicted 3D structure of the hnRNPL–*tRF-21* complex. $^{**}P < 0.01$ and $^{***}P < 0.001$, by 1-way ANOVA with Dunnett's T3 multiple-comparison test (**C**, **D**, and **H**).

when cells were treated with the AKT pathway agonist SC79 or with constitutive activation of AKT2 after *tRF-21* overexpression (Figure 4E). We also investigated the hnRNP L phosphorylation status in cells with AKT2 knockdown and found that p–hnRNP L levels were markedly lower than those in control cells. Furthermore, in cells with AKT2 knockdown, *tRF-21* overexpression slightly reduced p–hnRNP L levels, but *tRF-21* knockdown moderately increased p–hnRNP L levels, suggesting that there might be other kinases involved in this process (Supplemental Figure 4A). We further examined whether AKT1 participates in hnRNP L phosphorylation, and the results showed that in cells with *tRF-21* knockdown, silencing *AKT2* substantially reduced p-hnRNP L levels; however, knockdown of both AKT2 and AKT1 almost completely abolished hnRNP L phosphorylation, suggesting that AKT1 may also have some compensatory activity in hnRNP L phosphorylation (Supplemental Figure 4B). Together, these results clearly demonstrate that *tRF-21* prevented hnRNP L phosphorylation by AKT2/AKT1.

Since FISH and immunofluorescence assays showed differential localizations of *tRF-21* and p–hnRNP L in the cytoplasm and nuclei of PDAC cells (Figure 4F), we wanted to know whether *tRF-21* regulates the subcellular localization of hnRNP L. We

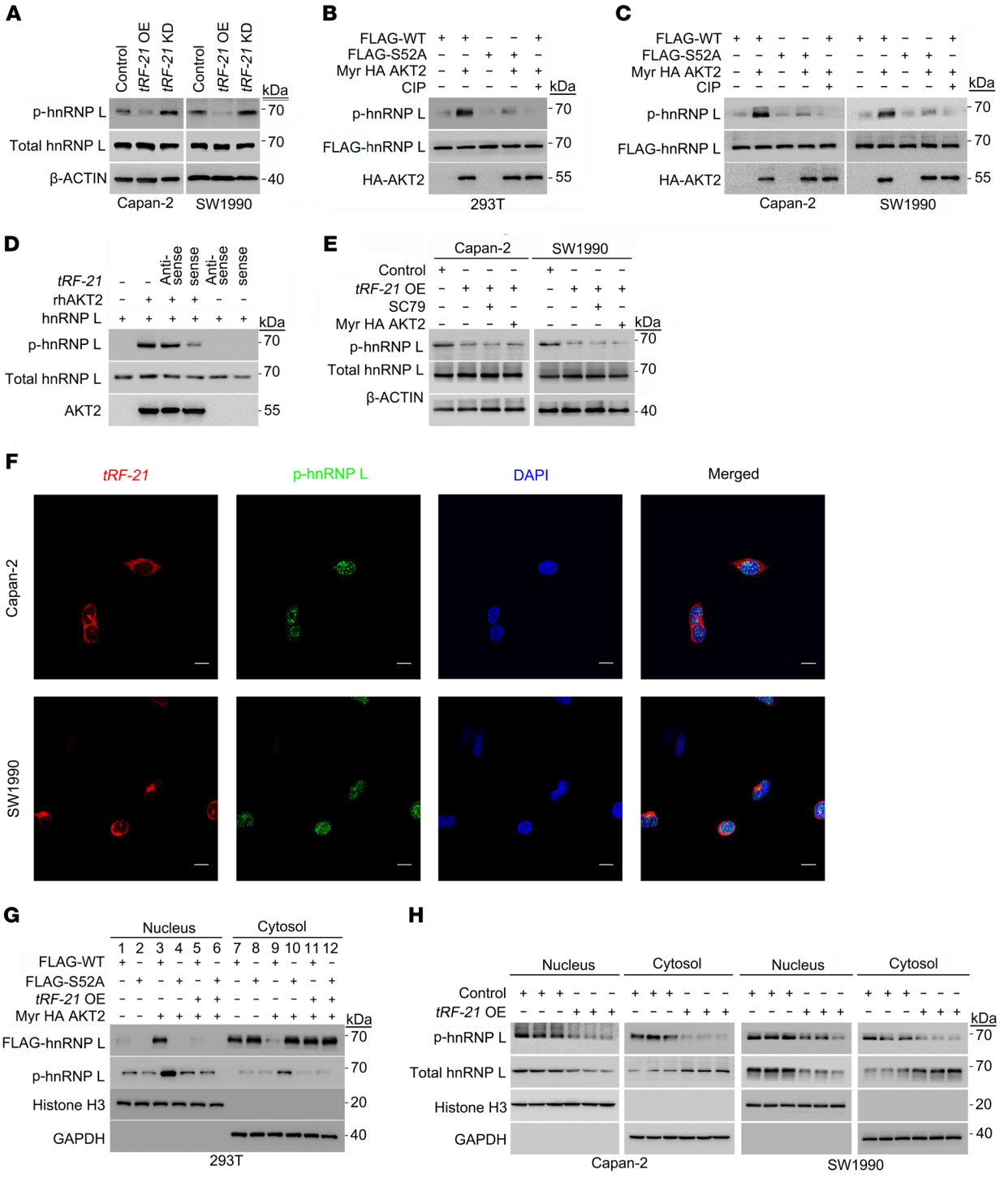

Figure 4. *tRF-21* suppresses the phosphorylation of hnRNP L at Ser52 by AKT2. (**A**) *tRF-21* expression changes altered p–hnRNP L levels. (**B** and **C**) Myr HA AKT2 phosphorylated FLAG–hnRNP L at Ser52 in 293T cells (**B**) and PDAC cells (**C**). Calf intestinal alkaline phosphate (CIP) was used for 1 hour at 37°C. (**D**) Effects of *tRF-21* sense or antisense on in vitro hnRNP L phosphorylation at Ser52 by recombinant human AKT2 (rhAKT2), showing that only *tRF-21* sense inhibited phosphorylation. hnRNP L was used as a loading control. (**E**) Effects of the AKT activator SC79 or Myr HA AKT2 on the phosphorylation of hnRNP L in the presence of *tRF-21*. SC79 (4 μg/mL) was added to incubate for 30 minutes. (**F**) FISH images for *tRF-21* and p–hnRNP L (*tRF-21*, red; p–hnRNP L, green). Cell nuclei were counterstained with DAPI. Scale bars: 10 μm. (**G**) Immunoblot analysis of p–hnRNP L and total hnRNP L localization in fractionated 293T cells transfected with FLAG–hnRNP L (FLAG-WT: lanes 1, 3, 5, 7, 9, and 11) or FLAG–S52A-mutant hnRNP L (FLAG-S52A: lanes 2, 4, 6, 8, 10, and 12) in the absence or presence of *tRF-21* (lanes 5, 6, 11, and 12) and Myr HA AKT2 (lanes 3, 4, 5, 6, 9, 10, 11, and 12). Histone H3 was used as a nuclear control, and GAPDH was used as a cytoplasmic control. (**H**) Immunoblot analysis of p–hnRNP L and total hnRNP L localization in fractionated PDAC cells stably overexpressing *tRF-21*. Histone H3 was used as a nuclear control, and GAPDH was used as a cytoplasmic control.

induced ectopic expression of FLAG-tagged Ser52–hnRNP L or FLAG-tagged Ala52–hnRNP L in 293T cells and then cotransfected them with Myr HA AKT2 or *tRF-21* and found that FLAG–Ser52–hnRNP L was present predominately in the cytoplasm (Figure 4G, lanes 1 and 7). However, induction of exogenous AKT2 promoted FLAG–Ser52–hnRNP L localization in the nucleus (Figure 4G, lanes 3 and 9). Interestingly, pretreatment of cells with *tRF-21* mimics before AKT2 induction retained FLAG–Ser52–hnRNP L in the cytoplasm, thereby abolishing the AKT2 effect (Figure 4G, lanes 5 and 11). In contrast, inducing exogenous AKT2 and increasing *tRF-21* in cells had no effect on FLAG–Ala52–hnRNP L localization (Figure 4G, lanes 2, 4, 6, 8, 10, and 12). We observed similar results in PDAC cells with increased *tRF-21* levels (Figure 4H). These results imply that subcellular distribution of hnRNP L depended on AKT2-mediated phosphorylation and that *tRF-21* was only involved in preventing hnRNP L phosphorylation.

tRF-21 represses hnRNP L–DDX17 complex formation. A previous study showed that activated hnRNP L is involved in alternative RNA splicing (26); however, the mechanism underlying this function has not been elucidated. We performed protein immunoprecipitation assays with an antibody against p–Ser52–hnRNP L followed by mass spectrometric analysis and identified 107 potential interacting proteins (Supplemental Table 3). Western blot analysis of the top 10 proteins ranked by the exponentially modified protein abundance index (emPAI) from the immunoprecipitation resultant showed that only DDX17 interacts with p–Ser52–hnRNP L (Figure 5, A and B). It has been shown that DDX17 protein has 2 isoforms, known as p82 and p72 (30, 31). On the basis of our Western blot analysis with the protein molecular size markers (Figure 5A), the DDX17 isoform that bound with p–hnRNP L was most likely p72. We then conducted immunoprecipitation assays using the antibody against DDX17 and cell lysates with or without phosphatase treatment to verify whether the interacting protein was p–Ser52–hnRNP L, and the result from Western blotting confirmed the presence of p–Ser52–hnRNP L (Figure 5C). Protein truncation mapping assays showed that it was the hnRNP L Gly-rich domain and the DDX17 helicase ATP-binding domain that interacted each other (Figure 5, D and E). Further experiments showed that decreasing *tRF-21* substantially promoted p–Ser52–hnRNP L and DDX17 interaction, which was abolished by treatment with phosphatase (Figure 5F). These results indicate that p–Ser52–hnRNP L could specifically bind DDX17 and that *tRF-21* was an important modulator for the interaction of these 2 proteins. To further clarify this function of *tRF-21*, we carried out immunoprecipitation assays using lysates from cells with ectopically expressed FLAG-tagged hnRNP L, and the results clearly showed binding of FLAG–hnRNP L to DDX17, and the binding was substantially enhanced by induction of AKT2 expression in cells; however, FLAG–Ala52–hnRNP L could not bind to DDX17, even in the presence of exogenous AKT2 (Figure 5G). These results demonstrate an essential role of the Ser52 residue in hnRNP L and its phosphorylation for the formation of an hnRNP L–DDX17 complex.

tRF-21 inhibits alternative splicing of Caspase 9 and mH2A1 pre-mRNAs. It has been shown that hnRNP L involves an alternative splicing of *Caspase 9* pre-mRNA (27, 28), which generates proapoptotic *Caspase 9a* and antiapoptotic *Caspase 9b* (Supplemental Figure 5A, upper panel), while DDX17 participates in alternative splicing of *mH2A1* (32), which generates anti-invasive *mH2A1.1* and proinvasive *mH2A1.2* in cancer cells (Supplemental Figure 5A, lower panel). We thus speculated that hnRNP L–DDX17 may be an RNA-splicing complex and jointly acts in *Caspase 9* and *mH2A1* alternative splicing. We found that cells silencing the expression of *HNRNPL* or *DDX17* had markedly increased ratios of *Caspase 9a*/*Caspase 9b* and *mH2A1.1*/*mH2A1.2* mRNAs compared with the corresponding control cells (Figure 6, A and B, and Supplemental Figure 5, B and C). Increasing the levels of *tRF-21* in cells had the same effect as silencing *HNRNPL* or *DDX17* expression, whereas decreasing the levels of *tRF-21* in cells substantially promoted formation of the antiapoptotic form of *Caspase 9b* and the proinvasive form of *mH2A1.2* (Figure 6, C–F). Since both *Caspase 9* and *mH2A1* play important roles in cancer malignancy and their activities are dependent on the alternative mRNA splicing induced by the hnRNP L–DDX17 complex that is postulated to be downstream of *tRF-21*, we carried out rescue experiments with PDAC cells. We found that decreasing *HNRNPL* and *DDX17* levels in cells silencing *tRF-21* expression significantly inhibited cell proliferation, migration, and invasion but promoted apoptosis (Supplemental Figure 5, D–G). In parallel, decreasing *HNRNPL* and *DDX17* expression restored the ratios of *Caspase 9a*/*Caspase 9b* and *mH2A1.1*/*mH2A1.2* mRNAs disturbed by the decreased levels of *tRF-21* in cells (Supplemental Figure 5, H and I). These results clearly demonstrate the functional role that *tRF-21* plays in inhibiting alternative splicing of *Caspase 9* and *mH2A1* pre-mRNAs through indirect inhibition of the hnRNP L–DDX17 complex.

Because KRAS, mutated in greater than 90% of PDACs, is a known upstream regulator of PI3K/AKT signaling (33), and AKT2 is a key kinase in the hnRNP L/CASP9/mH2A1 regulatory axis, we further examined the effect of *KRAS* silencing on AKT2 activation and, thus, the hnRNP L phosphorylation and downstream splicing effects on caspase 9a/b and mH2A1.1/2. The results clearly showed that silencing *KRAS* expression substantially decreased p–Ser474-AKT2 levels, which consequently led to a decrease in the levels of p–Ser52–hnRNP L, caspase 9b, and mH2A1.2, despite the fact that total AKT2 and hnRNP L levels remained unchanged and caspase 9a and mH2A1.1 levels were increased (Supplemental Figure 6A). These results indicate that KRAS is probably an upstream regulator in the AKT2/hnRNP L/caspase 9a/b/mH2A1.1/2 signaling axis. We thus examined the effects of *tRF-21* on this signaling axis in AKT2-amplified PANC-1 cells (34) and found that cells with *tRF-21* overexpression had substantially decreased levels of p–hnRNP L, caspase 9b, and mH2A1.2 but increased levels of caspase 9a and mH2A1.1 (Supplemental Figure 6B). These results demonstrate that *tRF-21* also works as a tumor suppressor in cells in the context of AKT2 amplification.

LIF or IL-6 inhibits tRF-21 formation mediated by SRSF5 in PADC cells. We next sought to determine why *tRF-21* production was significantly lower in PDAC tumor tissues than in normal tissues. Previous studies have reported that some cellular conditions such as hypoxia, oxidative stress, and nutritional starvation are involved in tRNA cleavage and tRF formation (23, 35). We thus examined their effects on *tRF-21* formation in vitro in PDAC cells and found that none of these conditions altered *tRF-21*

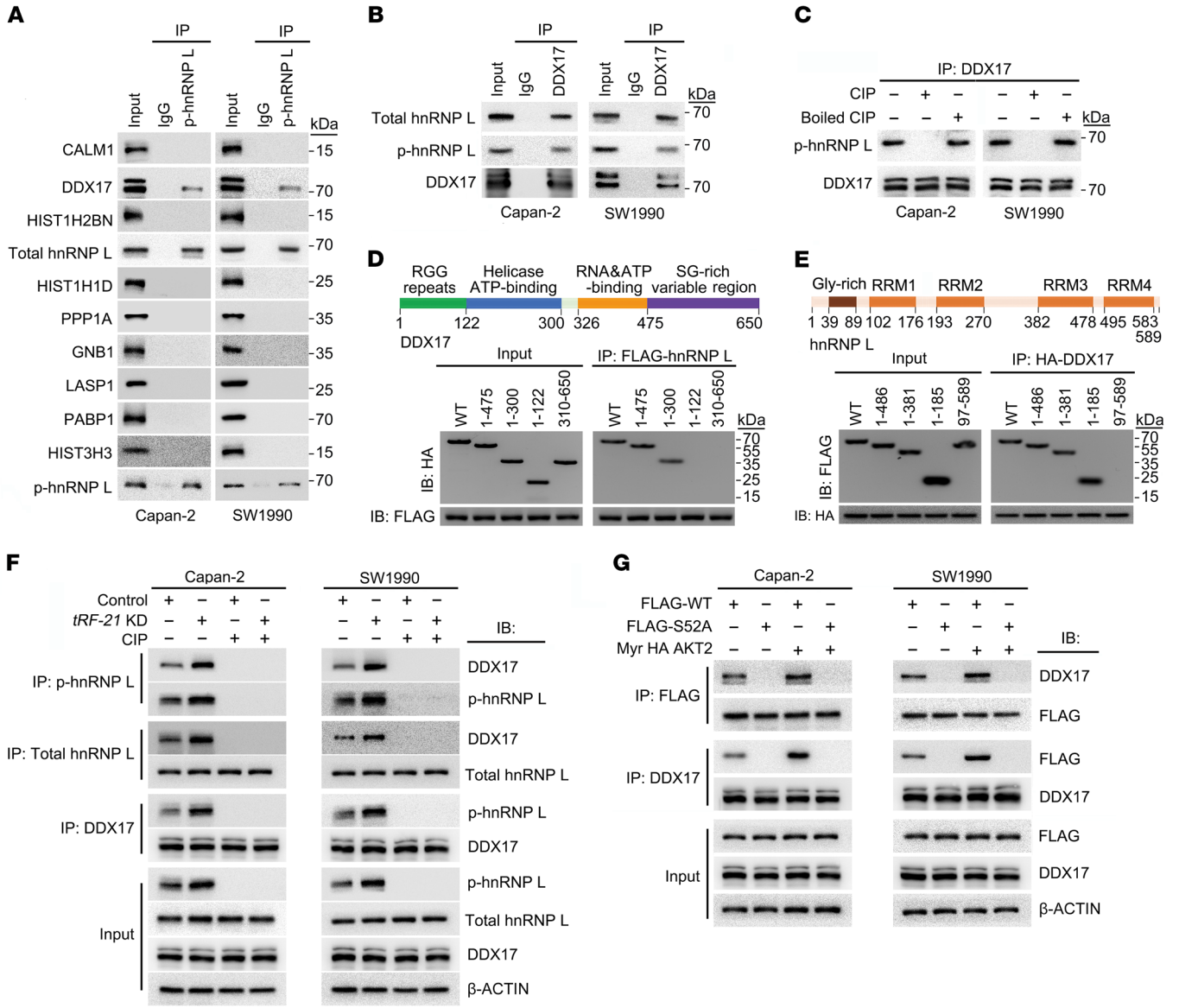

Figure 5. *tRF-21* inhibits p-Ser52-hnRNP L–DDX17 complex formation. (**A** and **B**) Reciprocal immunoprecipitation assays showed interaction of p-Ser52-hnRNP L (p-hnRNP L) with DDX17. (**C**) Immunoblot analysis of p-hnRNP L that coimmunoprecipitated with DDX17 in cells incubated with CIP or inactive CIP. (**D** and **E**) Truncation mapping of the interaction between hnRNP L and DDX17. Schematic diagrams show FLAG–hnRNP L (**D**) and HA-DDX17 (**E**) protein domain structures, respectively. Immunoblot analysis of the association of FLAG–hnRNP L constructs (full-length versus its truncated forms) and HA-DDX17 (**D**) or HA-DDX17 constructs (full-length versus its truncated forms) and FLAG–hnRNP L (**E**). (**F**) Reciprocal immunoprecipitation assays showed increased binding of p-hnRNP L and DDX17 upon *tRF-21* silencing. (**G**) Reciprocal immunoprecipitation assays showed the necessity of Ser52 phosphorylation for the interaction of hnRNP L with DDX17.

levels (Supplemental Figure 7, A–C). We therefore speculated that certain cytokines produced by inflammatory cells during PDAC initiation and progression might suppress *tRF-21* production. To test this notion, we assessed the effects on *tRF-21* formation of 5 inflammatory cytokines that play oncogenic roles in PDAC progression (7–14), including TNF-α, IL-1α, IL-6, and IL-10, secreted by macrophages and T cells in the TME (36), and LIF, produced by tumor cells and other microenvironmental cells such as pancreatic stellate cells (12). We found that treatment of PDAC cells with LIF or IL-6 significantly inhibited *tRF-21* production in a dose-dependent manner (Figure 7, A and B); however, treatment of cells with LIF or IL-6 preincubated with its neutralizing antibody did not affect *tRF-21* production (Figure 7C). Furthermore, we treated PDAC cells with a LIF-neutralizing antibody and found that *tRF-21* levels were reduced compared with levels in cells treated with nonspecific IgG or cells without treatment, indicating that PDAC cells themselves may produce LIF in an autocrine manner and inhibit *tRF-21* biogenesis (Supplemental Figure 7D). To elucidate why the 2 cytokines could inhibit *tRF-21* formation, we first performed in silico analysis with the online tool RBPmap (37) to search for RNA-binding proteins for mature $tRNA^{GlyGCC}$ that may produce *tRF-21* and found 8 candidates (Supplemental Table 4). We then respectively silenced these 8 proteins in PDAC cells to test their effect on *tRF-21* formation,

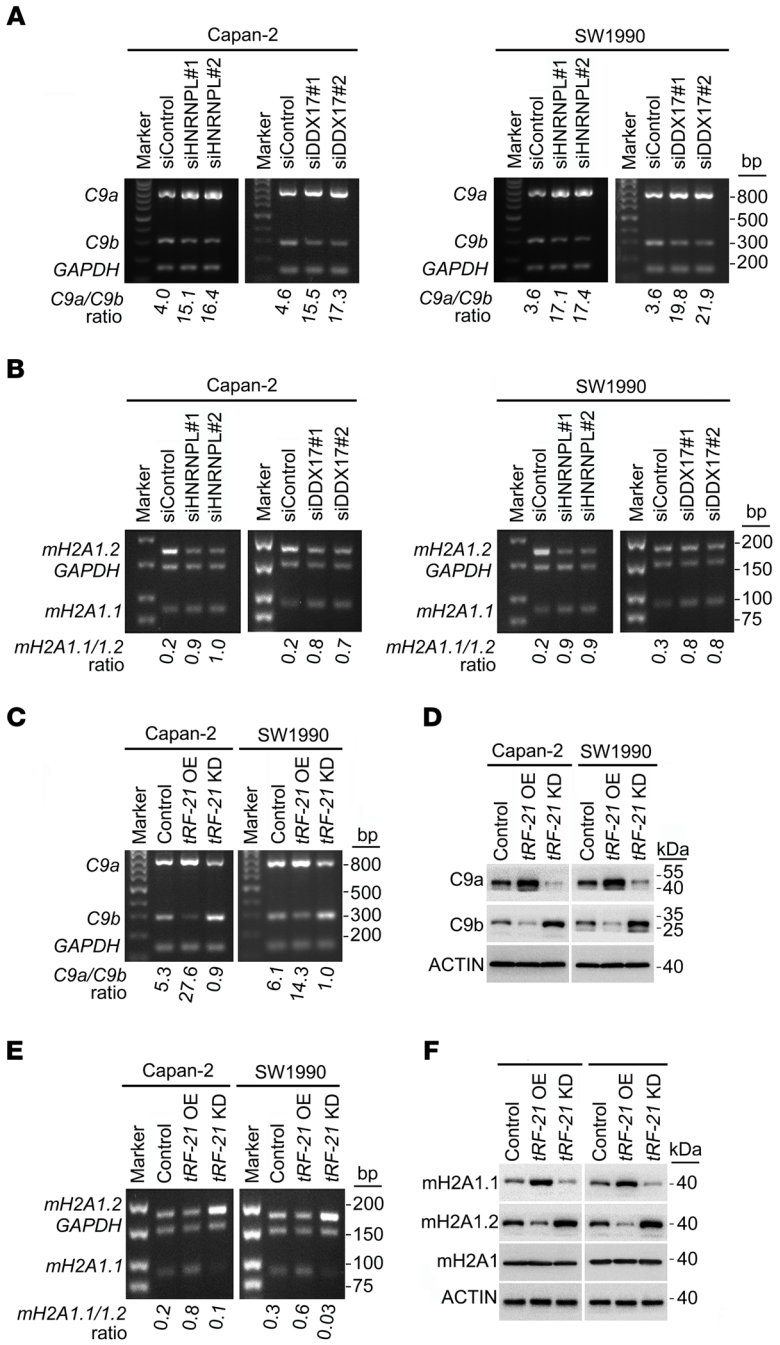

Figure 6. *tRF-21* facilitates *Caspase 9a* and *mH2A1.1* production via the p–Ser52–hnRNP L–DDX17 complex. (**A** and **B**) Semiquantitative RT-PCR showed upregulated ratios of *Caspase 9a/9b* (*C9a/C9b*) mRNAs (**A**) and *mH2A1.1/mH2A1.2* (*mH2A1.1/1.2*) mRNAs (**B**) when *HNRNPL* or *DDX17* was silenced. (**C** and **D**) Effects of *tRF-21* expression changes on alternatively spliced *Caspase 9* mRNA (**C**) and caspase 9a (C9a) and caspase 9b (C9b) protein (**D**) levels. (**E** and **F**) Effects of *tRF-21* expression changes on alternatively spliced *mH2A1* mRNA (**E**) and mH2A1 protein (**F**) levels.

and the results showed that it was *SRSF5* silencing that significantly reduced *tRF-21* levels (Figure 7D and Supplemental Figure 8A). Analysis of published individual nucleotide resolution UV crosslinking and immunoprecipitation (iCLIP-Seq) data (38) suggested that SRSF5 interacts with $tRNA^{GlyGCC}$ (Figure 7E). Consistently, qPCR analysis of the products of RIP with an antibody against SRSF5 verified the existence and accumulation of $tRNA^{GlyGCC}$ (Figure 7F). RNA-pulldown assays demonstrated that the RRM2 domain of SRSF5 was required for binding of SRSF5 and $tRNA^{GlyGCC}$ (Figure 7G). These results imply that SRSF5 was involved in generating *tRF-21* from $tRNA^{GlyGCC}$.

Next, we examined whether the cytokine-induced *tRF-21* decline was dependent on SRSF5 and, if so, how it functions. RIP assays using an antibody against SRSF5 showed that LIF or IL-6 treatment significantly decreased SRSF5 and $tRNA^{GlyGCC}$ binding in a dose-dependent manner (Figure 8A and Supplemental Figure 8B). Since LIF or IL-6 treatment significantly decreased *SRSF5* mRNA levels in cells (Figure 8B and Supplemental Figure 8C), we thought that the decreased binding of SRSF5 and $tRNA^{GlyGCC}$ could be due to a reduction in *SRSF5* expression. In silico analysis of the *SRSF5* promoter region (1000 bp from the *SRSF5* transcription start site [TSS]) using ChIPBase (39) and Gene Transcription Regulation Database (GTRD) (40) suggested that KLF4 may be a transcription factor involved in the regulation of *SRSF5* expression and that the *cis* element may be located between 184 and 193 bp downstream of the *SRSF5* TSS (Figure 8C). ChIP assays showed binding of KLF4 to the *SRSF5* promoter, and the binding was significantly enhanced by LIF or IL-6 treatment in a dose-dependent manner in PDAC cells (Figure 8, D–F). We hypothesized that the LIF- or IL-6–induced, KLF4-mediated *SRSF5* transcriptional repression was independent of KLF4 levels but relied on the ability of KLF4 to bind to the *SRSF5* promoter. To test this notion, we treated cells with the KLF4 expression promoter TNF-α (41, 42) and found that both mRNA and protein levels of KLF4 were indeed upregulated by TNF-α (Supplemental Figures 8, D and E); however, ChIP-qPCR assays showed that TNF-α treatment had no effect on KLF4 binding to the *SRSF5* promoter (Supplemental Figure 8F). Reporter gene assays showed that LIF or IL-6 treatment significantly repressed the transcriptional activity of the *SRSF5* promoter in a dose-dependent manner; however, silencing of KLF4 expression restored reporter gene expression. Moreover, mutations in the KLF4 binding site in the *SRSF5* promoter completely abolished the LIF or IL-6 effect, even under the condition of increased ectopic expression of KLF4 in cells (Supplemental Figure 8G). Overexpression of KLF4 in PDAC cells slightly, but not significantly, suppressed the *SRSF5* promoter activity compared with control under the condition of no LIF or IL-6 treatment (Supplemental Figure 8H). These results, together with our finding that LIF or IL-6 treatment significantly enhanced the binding of KLF4 to the *SRSF5* promoter but did not affect KLF4 levels (Figure 8, E and F, and Supplemental Figure 9A), suggest that KLF4 is a transcriptional repressor of *SRSF5* expression in PDAC cells but that this action may not depend on its level.

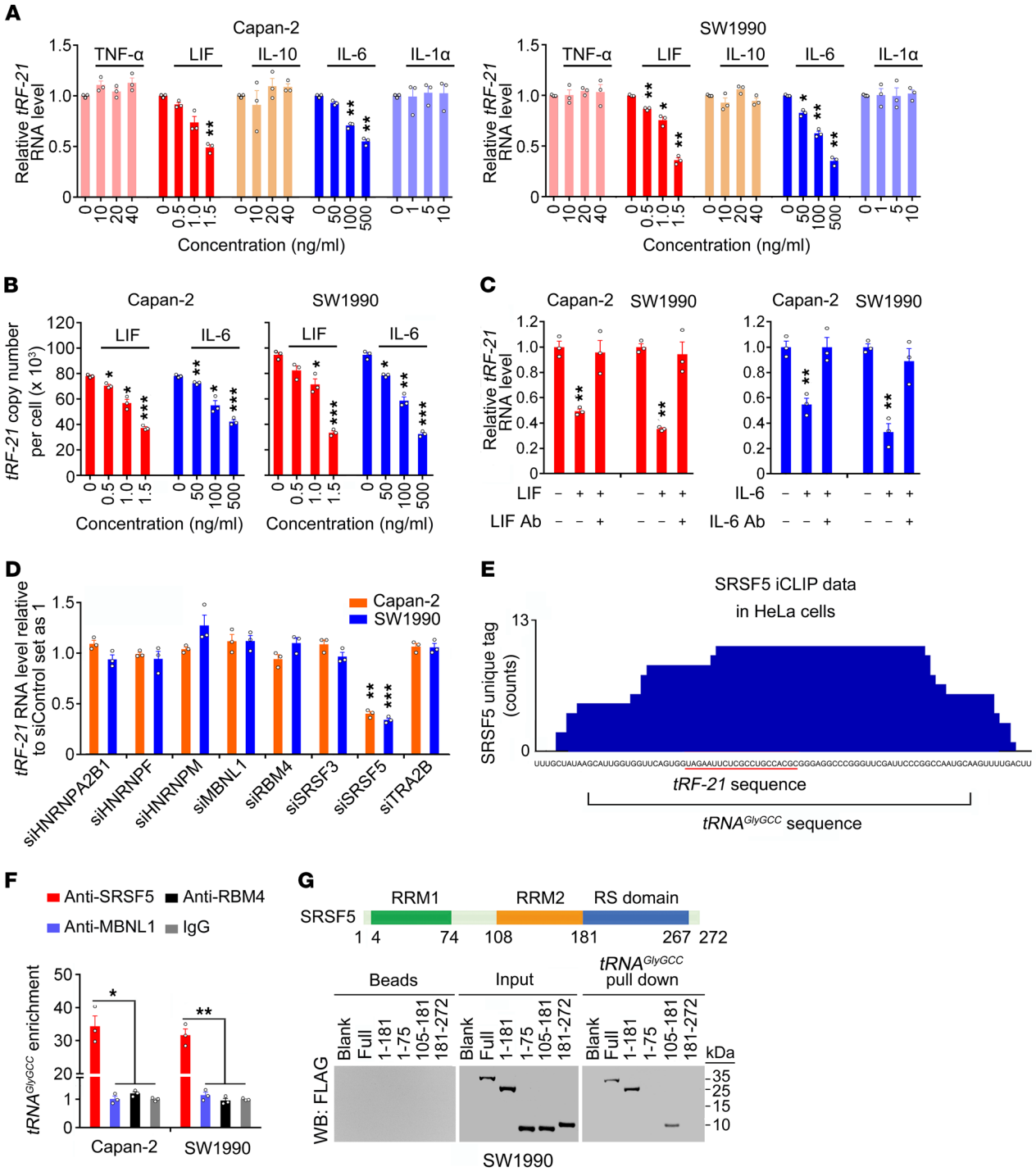

Figure 7. LIF and IL-6 inhibits *tRF-21* formation mediated by SRSF5. (**A**) *tRF-21* levels in PDAC cells cultured with inflammatory cytokines at different concentrations. The cytokines used in this study (TNF-α, LIF, IL-10, IL-6 and IL-1α) were dissolved in 0.5% BSA. (**B**) Absolute *tRF-21* copy numbers in PDAC cells treated with LIF or IL-6 at different concentrations. (**C**) *tRF-21* RNA levels in PDAC cells treated with LIF (1.5 ng/ml) or IL-6 (500 ng/mL) or the same amount of these cytokines neutralized by their antibody (LIF Ab, 2 μg/mL or IL-6 Ab, 80 μg/mL) for 1 hour before addition to the assay mixture. (**D**) *tRF-21* RNA levels in cells with silenced expression of RNA-binding proteins predicted by RBPmap to potentially interact with $tRNA^{GlyGCC}$. (**E**) Analysis of published SRSF5 iCLIP-Seq data showed that SRSF5 interacts with $tRNA^{GlyGCC}$. The *tRF-21* and $tRNA^{GlyGCC}$ sequences are underlined. (**F**) Association of SRSF5 with $tRNA^{GlyGCC}$ in PDAC cells as determined by RIP assays. IgG was used as a negative control. (**G**) Truncation mapping confirmed that $tRNA^{GlyGCC}$ interacted with the RRM2 domain of SRSF5. A diagram of the SRSF5 protein domain structure is shown. Immunoblot analysis shows FLAG-SRSF5 (Full) and its truncated forms pulled down by in vitro–transcribed biotinylated $tRNA^{GlyGCC}$. Data in **A**–**D** and **F** indicate the mean ± SEM of least 3 independent experiments. $^*P < 0.05$, $^{**}P < 0.01$, and $^{***}P < 0.001$, by 1-way ANOVA with Dunnett's T3 multiple-comparison test.

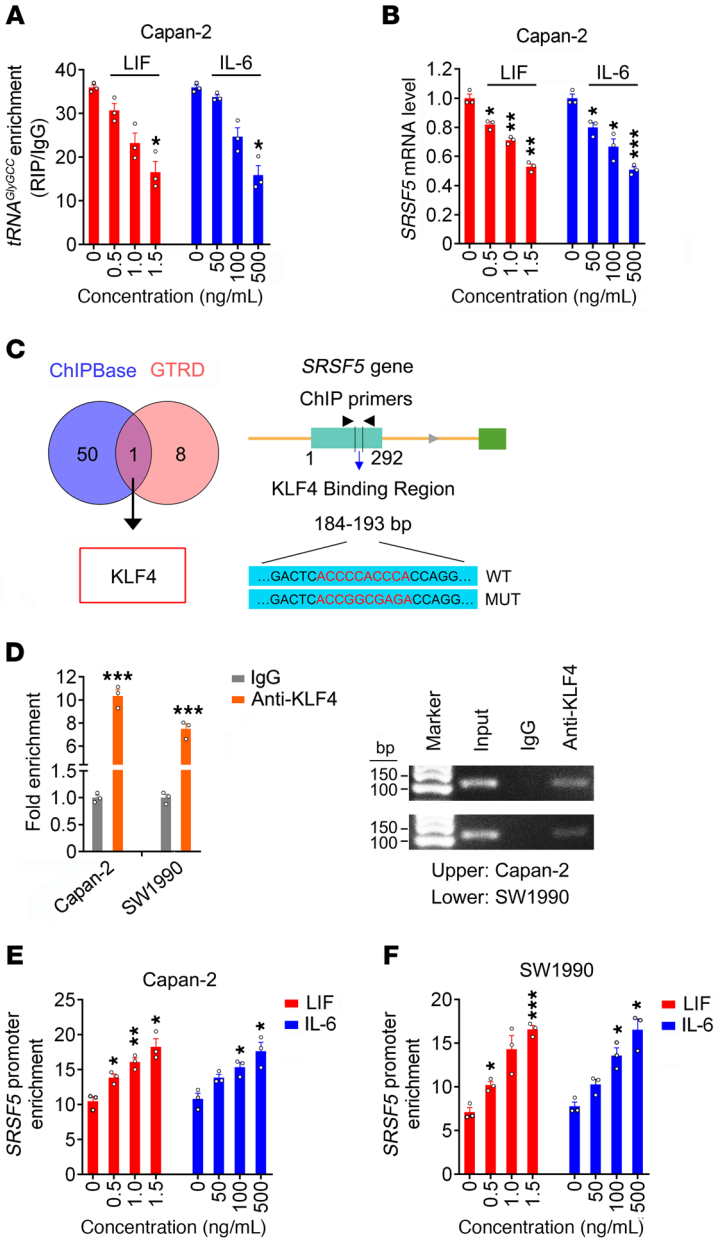

Figure 8. LIF or IL-6 enhances KLF4 binding to the *SRSF5* promoter region. (**A**) Association of SRSF5 with *tRNA*^{GlyGCC} determined by RIP assays in cells cultured with LIF or IL-6 at different concentrations. (**B**) *SRSF5* mRNA levels in cells treated with LIF or IL-6 at different concentrations. (**C**) Venn diagram of silico analysis of potential transcription factors in the *SRSF5* promoter region in cells (left panel). Schematic shows the putative KLF4 binding site in the promoter of the *SRSF5* gene and the primers used for ChIP analysis. The consensus and mutant sequences for KLF4 binding are highlighted. (**D**) ChIP assays using anti-KLF4 antibody or IgG control coupled with qPCR analysis. qPCR results are shown in the left panel, and agarose gel electrophoresis of the qPCR products is shown in the right panel. (**E** and **F**) KLF4 bound to the *SRSF5* promoter, as measured by ChIP assays in cells cultured with LIF or IL-6 at different concentrations in Capan-2 (**E**) and SW1990 (**F**) cell lines. Data in **A**, **B**, and **D**–**F** indicate the mean ± SEM of at least 3 independent experiments. **P* < 0.05, ***P* < 0.01, and ****P* < 0.001, by 1-way ANOVA with Dunnett's T3 multiple-comparison test (**A**, **B**, **E**, and **F**) and Student's *t* test (**D**).

We next performed rescue experiments to determine whether KLF4 is involved in regulating *tRF-21* production, and the results showed that decreasing KLF4 significantly increased the levels of both *SRSF5* and *tRF-21* in cells treated with LIF or IL-6 (Supplemental Figure 8I), indicating that KLF4 was responsible for *tRF-21* production. Analysis of protein expression in cells showed that treatment with LIF or IL-6 substantially decreased SRFS5 levels in a cytokine dose–dependent manner, without changing KLF4 levels; in parallel, the levels of p–Ser52–hnRNP L, caspase 9b, and mH2A1.2 were increased (Supplemental Figure 9A), similar to the effect seen with the decrease of *tRF-21* in cells. Furthermore, increasing *SRSF5* or *tRF-21* levels abolished the effect of LIF or IL-6 on this regulatory axis, and decreasing *tRF-21* substantially inhibited the effects of increased *SRSF5* (Supplemental Figure 9B).

Finally, we found that LIF or IL-6 treatment significantly promoted PDAC cell growth, migration, and invasion, but increasing *tRF-21* or silencing *HNRNPL* completely inhibited these malignant phenotypes caused by the cytokines (Supplemental Figures 10, A–D). These in vitro results were also observed in surgically removed primary tissues from patients with PDAC (n = 10). We found that the levels of *tRF-21* and SRSF5, caspase 9a, and mH2A1.1 proteins were all markedly lower in 10 tumors than in adjacent normal tissues; in contrast, the levels of p–Ser52–hnRNP L, caspase 9b, and mH2A1.2 proteins were substantially higher in tumors than in normal tissues (Supplemental Figure 10E). Moreover, we detected a negative correlation between *tRF-21* and *LIF* or *IL6* mRNA levels in 227 PDAC tumor tissues (Supplemental Figure 10F). These results demonstrated that the anti–PDAC progression effect of *tRF-21* probably occurred through the SRSF5/*tRF-21*/hnRNP L/caspase 9/mH2A1 regulatory axis, which can be repressed by inflammatory cytokines (Supplemental Figure 9C).

We then searched in TCGA database for correlations between *tRF-21* levels in cancer tissues and patient survival times for 9 types of common cancer and found a significant correlation only in PDAC: patients with high *tRF-21* levels in cancerous tissue survived longer than did patients with low *tRF-21* levels in cancerous tissue (log-rank P = 0.0035). However, the correlations were not significant in other cancer types such as esophageal carcinoma (ESCA), colon adenocarcinoma (COAD), liver hepatocellular carcinoma (LIHC), stomach adenocarcinoma (STAD), lung adenocarcinoma (LUAD), prostate adenocarcinoma (PRAD), and breast invasive carcinoma (BRCA), with the exception of lung squamous cell carcinoma (LUSC), in which high *tRF-21* levels seemed to be associated with shorter patient survival (Supplemental Figure 11). These results imply that the tumor suppressor role of *tRF-21* may be PDAC specific.

Therapeutic effect of tRF-21 in mouse xenograft and patient-derived xenograft models. Since *tRF-21* showed a strong anti-PDAC effect, we established models in which mice carried pancreatic xenografts derived from PDAC cells with *tRF-21* knockdown and treated the mice with *tRF-21* (Figure 9A). Mice that received agotRF-21 (40 mg/

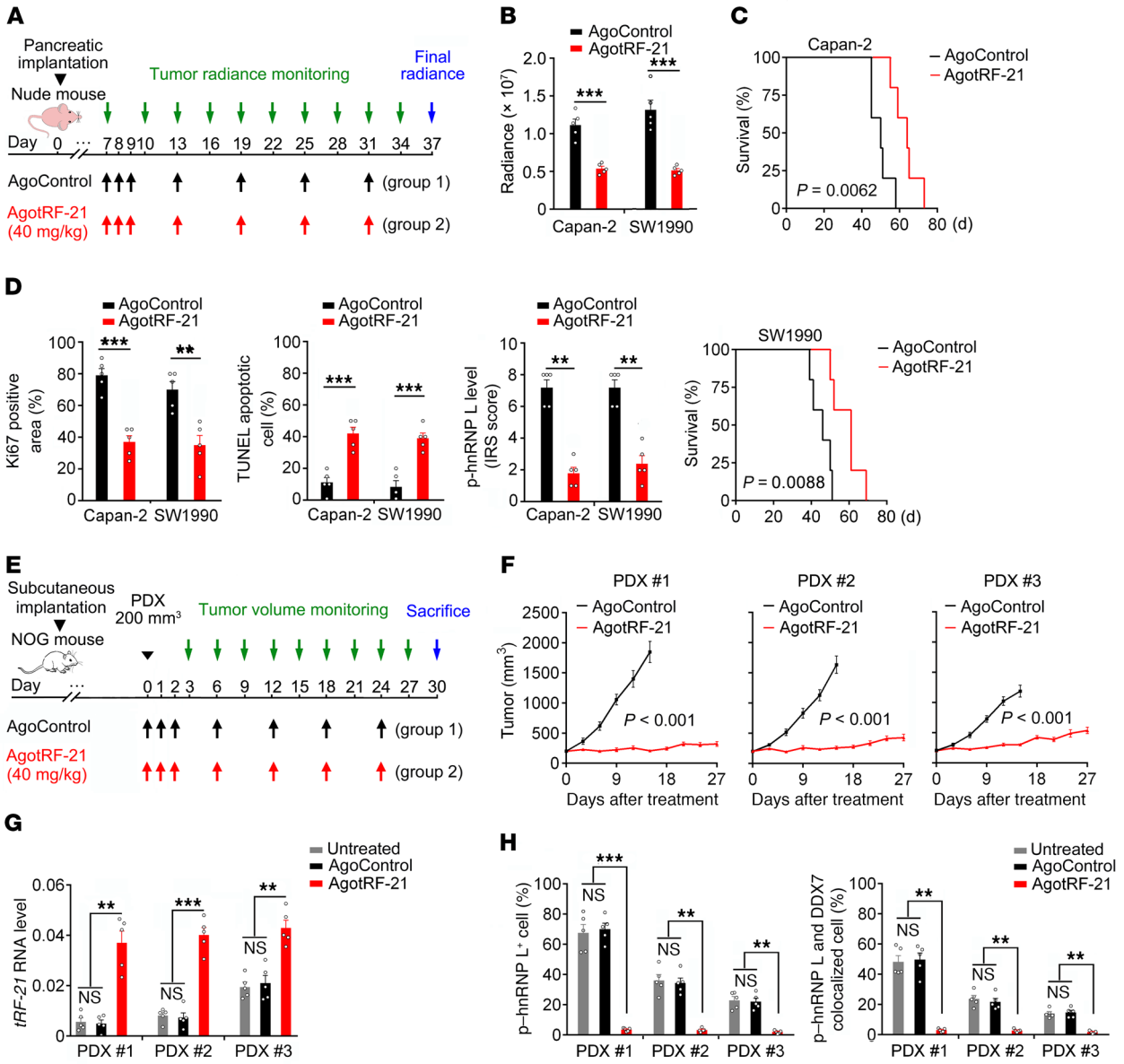

Figure 9. Therapeutic effect of *tRF-21* in mouse xenograft and PDX models. (**A**) Schematic for the treatment of mice carrying pancreatic xenografts derived from PDAC cells with *tRF-21* knockdown that were intravenously injected with agotRF-21 or agoControl. Colored arrows indicate dosing and tumor radiance monitoring time points. (**B** and **C**) Quantitative fluorescence intensity (**B**) and survival (**C**) analysis of mice according to treatment (n = 5 for each group). P values in **C** were calculated by log-rank test. (**D**) IHC analysis of Ki67-positive areas, TUNEL-positive apoptotic cells, and p–Ser52–hnRNP L (p–hnRNP L) levels in orthotopically implanted PDACs according to treatment type. Quantification of IHC staining. IRS, immune reactive score. (**E**) Schematic for the treatment of mice carrying a PDX that were treated with agotRF-21 or agoControl via intravenous injection. Colored arrows indicate the different treatments and tumor radiance monitoring time points. (**F**) AgotRF-21 treatment significantly inhibited PDX growth in mice. (**G**) *tRF-21* levels in PDXs of mice with different treatments. (**H**) Immunofluorescence analysis of p–hnRNP L and p–hnRNP L/DDX17 costaining in PDXs. Shown are the percentages of p–hnRNP L–positive cells and p–hnRNP L and DDX17 colocalized cells. Results in **B**, **D**, and **F**–**H** indicate the mean ± SEM of 5 mice per group. $^{**}P < 0.01$ and $^{***}P < 0.001$, by Student's t test (**B**, **D**, left and middle panels, and **F**); Wilcoxon test (**D**, right panel); and 1-way ANOVA with Dunnett's T3 multiple-comparison test (**G** and **H**).

kg, i.v.) had a significantly reduced tumor burden and longer survival than did mice that received control (agoControl) (Figure 9, B and C, and Supplemental Figure 12A). We found that mice that received agotRF-21 had 4-fold higher levels of *tRF-21* in their tumor tissues than did mice that received agoControl (Supplemental Figure 12C). IHC analysis revealed that, compared with agoControl treatment, agotRF-21 treatment significantly reduced Ser52-hnRNP L phosphorylation and cancer cell proliferation but promoted cancer cell apoptosis in xenografts (Figure 9D and Supplemental Figures 12B); however, cell proliferation in normal tissues such as intestines, where cells can be highly proliferative, was not affected (Supplemental Figures 12D). Interestingly, we found that tumor tissues from mice treated with agotRF-21 had similar STAT3 and p-STAT3 levels compared with tumor tissues from mice treated with agoControl (Supplemental Figure 12, E and F), implying that PDAC,

LIF, or IL-6 acted as *SRSF5* transcriptional suppressors that ultimately inhibited *tRF-21* formation but may not have functioned through the STAT3 signaling pathway. We also established mouse lung colonization models by injecting *tRF-21*–knockdown PDAC cells into the tail vein, and then treated the mice with agotRF-21 (40 mg/kg, i.v.) or agoControl (Supplemental Figure 13A). The mice that received agotRF-21 treatment had significantly reduced lung colonization of PDAC cells compared with those that received agoControl (Supplemental Figures 13, B and C).

To further examine the therapeutic effect of *tRF-21* mimics, we established PDX mouse models using tumor tissue from 3 patients with PDAC and treated the mice with agotRF-21 (Figure 9E). The results showed that PDXs in mice that received agotRF-21 (40 mg/kg, i.v.) had significantly reduced growth rates compared with those in mice treated with agoControl (Figure 9F and Supplemental Figure 14A). However, we found that the responses to the 3 PDXs were heterogeneous among the mice, which probably reflected the different levels of *tRF-21* expressed in these PDXs. We found that administration of agotRF-21 significantly increased *tRF-21* levels in the PDXs (Figure 9G) but did not affect body weights of the mice (Supplemental Figure 14B), suggesting that the agent had no apparent toxicity to the animals.

IHC analysis showed that administration of agotRF-21 significantly inhibited Ser52–hnRNP L phosphorylation and cancer cell growth but promoted apoptosis compared with untreated or agoControl-treated PDXs (Supplemental Figure 14, C and D). Consistent with the results seen with orthotopic xenograft models, administration of agotRF-21 did not affect intestinal cell proliferation or the levels of STAT3 and p-STAT3 in the PDXs (Supplemental Figures 14, E and F). Analysis of molecules downstream of *tRF-21* in PDXs revealed that agotRF-21 administration substantially increased the levels of caspase 9a and mH2A1.1 compared with levels in the untreated controls or in the controls treated with agoControl (Supplemental Figure 14G). We further performed dual-immunostaining assays and found that the proportions of p–Ser52–hnRNP L–positive cells and p–Ser52–hnRNP L– and DDX17-colocalized cells were significantly decreased in PDXs in mice treated with agotRF-21 compared with PDXs in untreated mice or mice treated with agoControl (Figure 9H and Supplemental Figure 15).

We next examined whether agotRF-21 has side effects in animals by treating 8-week-old BALB/c nude mice and NOG mice with various doses of agotRF-21. NOG mice are characterized by the absence of T and B lymphocytes and NK cells, insufficient function of macrophages and dendritic cells, and decreased activity of the complements. We found that with administration of up to 160 mg/kg agotRF-21, the mice showed no apparent signs of toxicity, as they maintained their body weight (Supplemental Figure 16A), steady-state hematopoiesis (Supplemental Figure 16, B–D), and liver and kidney function (Supplemental Figure 16, E–H). Together, these results demonstrate that agotRF-21 is a potential therapeutic agent for PDAC with no apparent toxicity.

Discussion

In the present study, we identified an inflammatory cytokine–regulated tRF, *tRF-21*, which is derived from $tRNA^{GlyGCC}$ by the splicing factor SRSF5. Our studies revealed that *tRF-21* acted as a tumor suppressor in the progression of PDAC: its levels were significantly lower in PDAC tumors than in nontumor tissues, and the decreased levels correlated with malignant phenotypes of PDAC cells and poor patient survival. Mechanistically, we have demonstrated that *tRF-21* bound Ser52 in the Gly-rich domain of the oncogenic RNA-binding protein hnRNP L and prevented the latter from phosphorylation by AKT2/1, which attenuated the formation of hnRNP L-DDX17, an alternative RNA splicing complex. Decreased *tRF-21* expression in PDAC cells in response to stimulation by certain inflammatory cytokines such as LIF and IL-6 may have enhanced hnRNP L–DDX17 activity, driving alternative splicing of *Caspase 9* and *mH2A1* pre-mRNAs to generate *Caspase 9b* and *mH2A1.2* that have respective antiapoptotic or proinvasive effects. We have also demonstrated that treatment of *tRF-21* mimics markedly repressed tumor cell colonization in the lungs and the growth of xenografts and PDXs in mice. These results shed light on a function of tRFs and suggest that *tRF-21* might be an effective therapeutic agent for PDAC.

Studies have shown that tRFs may function in multiple modes in cells. Like miRNA, some tRFs directly bind to the 3′-UTR region of target mRNA, resulting in translation repression (18–21). Other tRFs suppress the stability of some oncogene transcripts through displacing the 3′-UTR. For example, it has been reported that hypoxic conditions in breast cancer increase 4 i-tRFs, which repress the stability of multiple oncogene transcripts by YBX1 displacement (22). Moreover, some tRFs regulate the translation process by changing the conformation of mRNAs (23). The present study reveals, for the first time to our knowledge, that certain tRFs (i.e., *tRF-21*) could bind to protein and alter the phosphorylation and consequent function of the target protein. These findings expand our knowledge of the roles of endogenous tRFs in cellular physiopathological processes. It would be interesting to investigate whether this tRF can act on other important oncogenic proteins.

In the present study, we have linked *tRF-21* formation in PDAC cells to inflammatory cytokines in the PDAC TME. We found that, upon stimulation with LIF or IL-6, the transcriptional suppressor KLF4 bound to the promoter of the splicing factor *SRSF5* in a dose-dependent manner, thereby repressing *tRF-21* formation from $tRNA^{GlyGCC}$ in PDAC cells. These results imply that the regulation of tRF formation may be an important mechanism for inflammatory factors to promote the transformation of inflammation into cancer, since inflammatory cytokines are commonly present in the TME. Although the correlation between *tRF-21* levels and survival of patients with cancer in TCGA database appeared to be PDAC specific, further studies are warranted to determine how the universality and specificity of this tRF mechanism work to transform inflammation into cancer progression, since the survival time of patients with cancer can be influenced by many factors such as tumor stage at the time of diagnosis and treatment type.

As RNA splicing proteins, hnRNP L and DDX17 have been shown to participate in the alternative splicing of mRNAs produced by many genes including *Caspase 9* and *mH2A1* (32, 43). In the present study, we have demonstrated that p–Ser52–hnRNP L and DDX17 function in complex and that the activity of this mRNA splicing complex is regulated by *tRF-21*. Further, we

gained an insight into the molecular mechanism for the regulation of p–Ser52–hnRNP L–DDX17 complex formation by *tRF-21*. In the cytoplasm, *tRF-21* bound to hnRNP L and prevented hnRNP L activation via Ser52 phosphorylation by AKT2/1. However, when *tRF-21* formation was repressed in cells by certain stimuli such as inflammatory cytokines, activated p–Ser52–hnRNP L entered the nucleus to form the p–Ser52–hnRNP L–DDX17 complex. Since the p–Ser52–hnRNP L–DDX17 complex alternatively spliced *Caspase 9* mRNA, forming antiapoptotic *Caspase 9b* and *mH2A1* mRNA, thereby forming invasion-promoting *mH2A1.2*, one might expect that these 2 cancer hallmarks would result in a more malignant PDAC. Here, we identified an oncogenic pathway from inflammatory cytokines (e.g., LIF and IL-6) to the effective molecules (e.g., caspase 9b and mH2A1.2) that drives PDAC development and progression.

Because *tRF-21* showed a strong effect on the suppression of PDAC cell growth and invasion in vitro, we treated mice carrying cell line–derived or patient primary tumor–derived xenografts with agotRF-21, an in vivo–optimized *tRF-21* mimic. Interestingly, our results showed that treatment with agotRF-21 considerably repressed the tumor burden of orthotopically implanted xenografts, thus directly reflecting the therapeutic effects of this tRF on PDAC. Furthermore, treatment of mice carrying PDXs from 3 individual patients also showed the therapeutic value of *tRF-21*. Because a PDX maintains the fundamental genotypic features of primary cancer and recapitulates individual heterogeneity, the results may better predict drug activity (44). We found that all 3 PDXs were responsive to agotRF-21 treatment, although there were distinct differences in its effectiveness that were likely due to tumor heterogeneity, including varying levels of *tRF-21* in these PDXs. As expected, xenografts from patients with low endogenous *tRF-21* levels had a substantially better treatment response than did those with high *tRF-21* levels. Further observations revealed that PDXs with high *tRF-21* levels also had lower levels of p–Ser52–hnRNP L and p–Ser52–hnRNP L–DDX17 complex but higher levels of proapoptotic caspase 9a and anti-invasive mH2A1.1, indicating the presence of the *tRF-21*/hnRNP L/caspase 9/mH2A1 regulatory axis in such an intricate PDAC TME. Interestingly, we found that agotRF-21 treatment did not alter the levels of STAT3 or p-STAT3 in PDAC xenograft tissues, indicating that the antitumor effect of *tRF-21*, suppressed by LIF and IL-6, was independent of the canonical LIF/IL-6/STAT3 pathway but mediated by KLF4-regulated SRSF5. These results support our hypothesis that *tRF-21* may be a potential therapeutic agent for tumors such as PDAC with active inflammation in their microenvironment.

Although we believe our study provides advances in the field, it has several limitations. First, this study focused on *tRF-21* and PDAC; whether other tRFs have the same effect on PDAC and whether *tRF-21* has the same role in other types of cancer remain unclear. Although the survival correlation analysis suggested that the levels of *tRF-21* in tumor tissues might not associate with survival time in patients with cancer other than PDAC in TCGA database, further molecular studies are warranted. Second, although we examined 5 cytokines and showed that LIF and IL-6 repressed *tRF-21* formation in PDAC cells, the effects of other cancer-related cytokines are not yet known. Therefore, it would be interesting to explore the roles of other cytokines produced by inflammation or other stress in the TME. Third, KLF4 is a well-known transcription factor that acts as a transcriptional activator or repressor, depending on the cellular context (45, 46). Our results indicate that in PADC cells treated with LIF or IL-6, suppression of *SRSF5* transcription by KLF4 was not dependent on KLF4 levels, implying that there might be other factors, such as posttranslational modifications of KFL4 itself (i.e., acetylation and PARylation; refs. 47, 48), or chromosome and DNA modifications, on the other hand, that determine KLF4 activity in regulating its target gene transcription. It would be interesting to identify the factor(s) that promote KLF4 to bind the *SRSF5* promoter upon simulation with LIF or IL-6. In addition in this study, we investigated the effects of changes in *tRF-21* expression levels on PDAC growth and colonization in immunocompromised mice; however, it would be necessary to verify these effects in immunocompetent mouse models as well. Finally, it should be noted that, in the present study, we examined only the alternative splicing of *Caspase 9* and *mH2A1* mRNAs. However, the p–Ser52–hnRNP L–DDX17 complex probably has other targets that need to be explored.

In conclusion, we have identified a tRF, *tRF-21*, that plays an important role in PDAC development and progression and shed light on the molecular mechanism underlying the effects of *tRF-21* on the suppression of PDAC growth and metastasis. The notable therapeutic effects achieved with treatment with synthetic *tRF-21* mimics in mice carrying PDAC cell line–derived xenografts or PDXs further verified the role of *tRF-21* in PDAC and suggest that this tRF is a potential therapeutic agent.

Methods

Study participants and clinical specimens. This study included 227 patients with PDAC recruited at Sun Yat-sen Memorial Hospital, Sun Yat-sen University (cohort 1, $n = 158$) and Cancer Hospital Chinese Academy of Medical Sciences (cohort 2, $n = 69$; Beijing, China) between 2005 and 2018 (Supplemental Table 5). PDAC was diagnosed by histopathological examination, and the patients' clinical characteristics were acquired from medical records. All patients underwent pancreatectomy, and none of them received chemotherapy or radiotherapy before surgery. The survival time of patients was defined as the date of the cancer diagnosis until the date of the last follow-up or death. Whether and when a patient died was determined from inpatient and outpatient records, the patient's family, or follow-up telephone calls. Each patient donated PDAC and the corresponding adjacent normal tissue samples at the time of pancreatectomy, and the samples were immediately frozen and stored in liquid nitrogen until use.

Analysis of publicly available data. See the Supplemental Methods for details.

In silico analysis. See the Supplemental Methods for details.

Cell lines and cell culturing. Capan-2, SW1990, and 293T cell lines were purchased from the Cell Bank of the Type Culture Collection of the Chinese Academy of Sciences, Shanghai Institute of Biochemistry and Cell Biology. See the Supplemental Methods for details.

Transient transfection of tRF-21 mimics, siRNAs, and plasmids. See the Supplemental Methods for details as well as Supplemental Table 6 for information on the *tRF-21* mimics and siRNAs used.

Northern blot assays. See the Supplemental Methods for details, including *tRF-21* probe labeled with digoxigenin from BersinBio in Supplemental Table 7.

qRT-PCR and four-leaf clover qRT-PCR analysis. See the Supplemental Methods for details, as well as Supplemental Table 7 for primer pair sequences, SL-adapter, and TaqMan probe used for $tRNA^{GlyGCC}$.

Measuring absolute tRF-21 copy numbers in cells. See the Supplemental Methods for details.

Subcellular fractionating. See the Supplemental Methods for details.

Lentivirus production and transduction and plasmid construction. Lentivirus-mediated *tRF-21* expression or silencing was achieved by the documented method with some modifications. Please see the Supplemental Methods for details.

Analysis of cell malignant phenotypes. See the Supplemental Methods for details about cell viability and apoptosis and cell invasion and migration assays.

RNA-pulldown assays. See the Supplemental Methods for details.

Protein immunoprecipitation. See the Supplemental Methods for details.

Mass spectrometric analysis. See the Supplemental Methods for details as well as the list of proteins ranked by the emPAI in Supplemental Tables 2 and 3.

Cell lysis and Western blot analysis. See the Supplemental Methods for details as well as the list of antibodies used in Supplemental Table 8 (see the full, uncut gels in Supplemental Figure 17).

RIP assays. RIP assays were performed using the Magna RIP RNA-Binding Protein Immunoprecipitation kit (MilliporeSigma, 17-700). See the Supplemental Methods for details.

ChIP assays. ChIP assays were performed using the EZ-Magna ChIP A/G Kit (17-10086, MilliporeSigma). See the Supplemental Methods for details.

IHC staining. See the Supplemental Methods for details.

RNA FISH and immunofluorescence. FISH was performed using the Ribo Fluorescent In Situ Hybridization Kit (RiboBio). See the Supplemental Methods for details.

In vitro Ser52–hnRNP L phosphorylation. Phosphorylation of Ser52–hnRNP L was performed in a mixture (20 μL) containing adequate amounts of synthesized *tRF-21* or its antisense, 80 ng recombinant hnRNP L (Abnova, H00003191-P01), 10 mM HEPES, 5 mM DTT, 120 mM KCl, 3 mM $MgCl_2$, 5% glycerol, 0.5 mM ATP, 1.25 mM glycerol-2-phosphate, and 200 ng recombinant human AKT2 (Abcam, ab79798). The mixture was incubated at 30°C for 30 minutes and then analyzed for p–Ser52–hnRNP L levels by Western blotting.

Stress formation and cytokine treatment of PDAC cells. Details on stress production and cytokine treatment are described in the Supplemental Methods.

Reporter gene assays. Reporter gene assays were conducted as described in the Supplemental Methods.

Establishment of mouse xenograft models. Four-week-old female BALB/c nude mice were obtained from Beijing Vital River Laboratory Animal Technology and allowed to acclimate to local conditions for 1 week under a 12-hour light/12-hour dark cycle, with adequate food and water. We established 4 different kinds of PDAC xenograft models. For the subcutaneous xenograft model, mice were subcutaneously injected in the back flank with 0.1 mL of a cell suspension containing 2×10^6 PDAC cells. When a tumor was palpable, it was measured every other day, and its volume was calculated according to the formula: volume = 0.5 × length × width^2. For the pancreatic xenograft model, luciferase-labeled PDAC cells (2×10^6) with stable expression of *tRF-21* or silenced *tRF-21* or control cells were surgically injected into the pancreas of female athymic nude mice. Tumor volumes were monitored by bioluminescence imaging using a Living Image system (PerkinElmer). For the PDX model, surgically removed fresh PDAC tissues from patients were propagated as subcutaneous tumors in 4-week-old NOG mice (Beijing Vital River Laboratory Animal Technology). Xenografts from these F1 mice were then cut into small pieces and subcutaneously implanted into other mice (F2 mice). When the xenografts reached a size of 1500 mm^3, they were excised, cut into small pieces, and transplanted again into F3 mice. For the lung metastatic or localization models, luciferase labeled PDAC cells with *tRF-21* stable knockdown (1×10^6) were injected into the tail vein of female athymic nude mice (49). Pulmonary tumor cell colonization was monitored by bioluminescence imaging.

Treatment of PDAC xenografts with tRF-21 mimic. We performed treatment with *tRF-21* mimics in mice carrying a pancreatic xenograft, lung-colonized tumors, or a PDX. Single-stranded *tRF-21* was synthesized with 2 phosphorothioates at the 5′ end, 4 phosphorothioates and 1 cholesterol group at the 3′ end, and 1 full-length nucleotide 2′-methoxy modification. We determined the dosage on the basis of previous studies (50–52) and pilot animal experiments. For mice with pancreatic xenografts, 7 days after implantation of PDAC cells with *tRF-21* stable knockdown, the mice were randomly divided into 2 groups (n = 5 per group) and treated with agotRF-21 in saline (40 mg/kg, i.v.) or the same amount of agoControl in saline (Supplemental Table 6). Treatment was administered every day for 3 days and then every 6 days, 4 times. Tumor burden was monitored every 3 days by bioluminescence imaging. Mice with lung colonization were randomly assigned to 2 groups (n = 5 per group) 1 day after the inoculation of PDAC cells with *tRF-21* stable knockdown and were given the same treatment as the pancreatic implantation animals. Lung colonization was monitored every 3 days by bioluminescence imaging. For the PDX models, when the xenografts reached approximately 200 mm^3 in size, the mice were randomly divided into 2 groups (n = 5 per group) and received the same treatment as the pancreatic implantation animals. Tumor volumes were monitored every 3 days and are expressed as 0.5 × length × width^2. Mice were sacrificed 6 days after the last treatment.

agotRF-21 toxicity test in mice. Female BALB/c nude mice and NOG mice were respectively divided into 7 groups (n = 5 per group) and treated with saline, agotRF-21 (40 mg/kg, 80 mg/kg, or 160 mg/kg body weight), or the same amount of agoControl in the same volume of saline. Caudal vein injection was performed every day for 3 days and then every 6 days, 4 times. Body weight was measured every 3 days, and blood samples were taken on the last day of treatment. Whole blood was diluted to measure the proportions of white blood cells, hemoglobin, and platelets using an automatic blood cell analyzer (Mindray). Serum levels of alanine transaminase and aspartate aminotransferase, indicating liver toxicity, and blood creatinine and urea nitrogen, indicating kidney toxicity, were analyzed in a Cobas 8000 automatic biochemical analyzer (Roche).

Statistics. We used the Student's t test to analyze the significance of differences between 2 means. To compare several groups, 1-way ANOVA with Dunnett's T3 multiple-comparison test was used. Fisher's exact test was used for any independence test between 2 categorical variables, and the Wilcoxon rank-sum test was used for any independence test between a continuous variable and a binary categorical variable, when there was no covariate to adjust for.

We used the log-rank test for univariate survival analyses and the Cox proportional hazards model in multivariate survival analyses. Kaplan-Meier plots are used to present the survival data. Spearman's rank correlation was used to test the correlation between the levels of the molecules of interest. All statistical analyses were performed using SPSS software, version 24.0 (IBM SPSS). A *P* value of less than 0.05 was considered significant for all statistical analyses, and the FDR was used to adjust multiple-comparison testing.

Study approval. Informed consent was obtained from each participant for use of their clinical specimens, and this study was approved by the IRBs of Sun Yat-sen Memorial Hospital, Sun Yat-sen University, and the Cancer Hospital Chinese Academy of Medical Sciences. All animal experiments were approved by the IACUC of Sun Yat-sen University Cancer Center.

Author contributions

J Zheng and DL conceptualized and supervised the study. LP and XH performed phenotypic and functional experiments. ZL and YY conducted statistical and bioinformatics analyses. RL, GW, LW, YZ JS, JD, SD, C Wu, XC, C Wang, and RC were responsible for sample preparation, clinical data collection, and association analyses. J Zhang, RB, and L Zhuang provided technical support. ML, L Zeng, and SZ contributed to histopathological analyses. J Zheng, LP, XH, and DL prepared the manuscript. All authors reviewed the manuscript.

Acknowledgments

This study was supported by the Natural Science Foundation of China (82072617 and 81772586, to J Zheng; 81802407, to XH; and 82003162, to J Zhang); the Program for Guangdong Introducing Innovative and Entrepreneurial Teams (2017ZT07S096, to DL); the Natural Science Foundation of Guangdong Province (2018A030313327, to XH); and Sun Yat-sen University Cancer Center Intramural Funds (to DL and J Zheng).

Address correspondence to: Jian Zheng or Dongxin Lin, Sun Yat-sen University Cancer Center, 651 Dongfeng East Road, Guangzhou 510060, China. Phone: 8620.8734.2346; Email: zhengjian@sysucc.org.cn (JZ); Phone: 8620.8734.2298; Email: lindx@sysucc.org.cn (DL).

1. Siegel RL, et al. Cancer statistics, 2020. *CA Cancer J Clin*. 2020;70(1):7–30.
2. Chen W, et al. Cancer statistics in China, 2015. *CA Cancer J Clin*. 2016;66(2):115–132.
3. Hanahan D, Weinberg RA. Hallmarks of cancer: the next generation. *Cell*. 2011;144(5):646–674.
4. Padoan A, et al. Inflammation and pancreatic cancer: focus on metabolism, cytokines, and immunity. *Int J Mol Sci*. 2019;20(3):676.
5. Guerra C, et al. Chronic pancreatitis is essential for induction of pancreatic ductal adenocarcinoma by K-Ras oncogenes in adult mice. *Cancer Cell*. 2007;11(3):291–302.
6. McAllister F, et al. Oncogenic Kras activates a hematopoietic-to-epithelial IL-17 signaling axis in preinvasive pancreatic neoplasia. *Cancer Cell*. 2014;25(5):621–637.
7. Wei D, et al. KLF4 is essential for induction of cellular identity change and acinar-to-ductal reprogramming during early pancreatic carcinogenesis. *Cancer Cell*. 2016;29(3):324–338.
8. Lesina M, et al. Stat3/Socs3 activation by IL-6 transsignaling promotes progression of pancreatic intraepithelial neoplasia and development of pancreatic cancer. *Cancer Cell*. 2011;19(4):456–469.
9. Zhang Y, et al. Interleukin-6 is required for pancreatic cancer progression by promoting MAPK signaling activation and oxidative stress resistance. *Cancer Res*. 2013;73(20):6359–6374.
10. Biffi G, et al. IL1-induced JAK/STAt signaling is antagonized by TGFβ to shape CAF heterogeneity in pancreatic ductal adenocarcinoma. *Cancer Discov*. 2019;9(2):282–301.
11. Ling JH, et al. KrasG12D-induced IKK2/β/NF-κB activation by IL-1α and p62 feedforward loops is required for development of pancreatic ductal adenocarcinoma. *Cancer Cell*. 2012;21(1):105–120.
12. Shi Y, et al. Targeting LIF-mediated paracrine interaction for pancreatic cancer therapy and monitoring. *Nature*. 2019;569(7754):131–135.
13. Bressy C, et al. LIF drives neural remodeling in pancreatic cancer and offers a new candidate biomarker. *Cancer Res*. 2018;78(4):909–921.
14. Shen L, et al. Local blockade of interleukin 10 and C-X-C motif chemokine ligand 12 with nanodelivery promotes antitumor response in murine cancers. *ACS Nano*. 2018;12(10):9830–9841.
15. Cole C, et al. Filtering of deep sequencing data reveals the existence of abundant Dicer-dependent small RNAs derived from tRNAs. *RNA*. 2009;15(12):2147–2160.
16. Su Z, et al. Angiogenin generates specific stress-induced tRNA halves and is not involved in tRF-3-mediated gene silencing. *J Biol Chem*. 2019;294(45):16930–16941.
17. Lee YS, et al. A novel class of small RNAs: tRNA-derived RNA fragments (tRFs). *Genes Dev*. 2009;23(22):2639–2649.
18. Sun C, et al. Roles of tRNA-derived fragments in human cancers. *Cancer Lett*. 2018;414:16–25.
19. Kuscu C, et al. tRNA fragments (tRFs) guide Ago to regulate gene expression post-transcriptionally in a Dicer-independent manner. *RNA*. 2018;24(8):1093–1105.
20. Zhong F, et al. Complement C3 activation regulates the production of tRNA-derived fragments Gly-tRFs and promotes alcohol-induced liver injury and steatosis. *Cell Res*. 2019;29(7):548–561.
21. Maute RL, et al. tRNA-derived microRNA modulates proliferation and the DNA damage response and is down-regulated in B cell lymphoma. *Proc Natl Acad Sci U S A*. 2013;110(4):1404–1409.
22. Huang B, et al. tRF/miR-1280 suppresses stem cell-like cells and metastasis in colorectal cancer. *Cancer Res*. 2017;77(12):3194–3206.
23. Goodarzi H, et al. Endogenous tRNA-derived fragments suppress breast cancer progression via YBX1 displacement. *Cell*. 2015;161(4):790–802.
24. Kim HK, et al. A transfer-RNA-derived small RNA regulates ribosome biogenesis. *Nature*. 2017;552(7683):57–62.
25. Pliatsika V, et al. MINTbase v2.0: a comprehensive database for tRNA-derived fragments that includes nuclear and mitochondrial fragments from all The Cancer Genome Atlas projects. *Nucleic Acids Res*. 2018;46(d1):D152–D159.
26. Hui J, et al. HnRNP L stimulates splicing of the eNOS gene by binding to variable-length CA repeats. *Nat Struct Biol*. 2003;10(1):33–37.
27. Goehe RW, et al. hnRNP L regulates the tumorigenic capacity of lung cancer xenografts in mice via caspase-9 pre-mRNA processing. *J Clin Invest*. 2010;120(11):3923–3939.
28. Vu NT, et al. hnRNP U enhances caspase-9 splicing and is modulated by AKT-dependent phosphorylation of hnRNP L. *J Biol Chem*. 2013;288(12):8575–8584.
29. Lim CY, et al. Tropomodulin3 is a novel Akt2 effector regulating insulin-stimulated GLUT4 exocytosis through cortical actin remodeling. *Nat Commun*. 2015;6:5951.
30. Uhlmann-Schiffler H, et al. The mRNA of DEAD box protein p72 is alternatively translated into an 82-kDa RNA helicase. *J Biol Chem*. 2002;277(2):1066–1075.
31. Hirai Y, et al. Differential roles of two DDX17 isoforms in the formation of membraneless organelles. *J Biochem*. 2020;168(1):33–40.
32. Dardenne E, et al. Splicing switch of an epigenetic regulator by RNA helicases promotes tumor-cell invasiveness. *Nat Struct Mol Biol*. 2012;19(11):1139–1146.
33. Buscail L, et al. Role of oncogenic KRAS in the diagnosis, prognosis and treatment of pancreatic cancer. *Nat Rev Gastroenterol Hepatol*. 2020;17(3):153–168.
34. Pettazzoni P, et al. Genetic events that limit the efficacy of MEK and RTK inhibitor therapies in a mouse model of KRAS-driven pancreatic cancer. *Cancer Res*. 2015;75(6):1091–1101.
35. Thompson DM, Parker R. Stressing out over tRNA cleavage. *Cell*. 2009;138(2):215–219.
36. Briukhovetska D, et al. Interleukins in cancer: from biology to therapy. *Nat Rev Cancer*. 2021:1–19.
37. Paz I, et al. RBPmap: a web server for mapping binding sites of RNA-binding proteins. *Nucleic*

Acids Res. 2014;42(web server issue):W361–W367.
38. Krchnakova Z, et al. Splicing of long non-coding RNAs primarily depends on polypyrimidine tract and 5' splice-site sequences due to weak interactions with SR proteins. *Nucleic Acids Res*. 2019;47(2):911–928.
39. Zhou KR, et al. ChIPBase v2.0: decoding transcriptional regulatory networks of non-coding RNAs and protein-coding genes from ChIP-seq data. *Nucleic Acids Res*. 2017;45(d1):D43–D50.
40. Yevshin I, et al. GTRD: a database on gene transcription regulation-2019 update. *Nucleic Acids Res*. 2019;47(d1):D100–D105.
41. Feinberg MW, et al. Kruppel-like factor 4 is a mediator of proinflammatory signaling in macrophages. *J Biol Chem*. 2005;280(46):38247–38258.
42. Wang B, et al. Krüppel-like factor 4 induces apoptosis and inhibits tumorigenic progression in SK-BR-3 breast cancer cells. *FEBS Open Bio*. 2015;5:147–154.
43. Fei T, et al. Genome-wide CRISPR screen identifies HNRNPL as a prostate cancer dependency regulating RNA splicing. *Proc Natl Acad Sci U S A*. 2017;114(26):E5207–E5215.
44. Garrido-Laguna I, et al. Tumor engraftment in nude mice and enrichment in stroma- related gene pathways predict poor survival and resistance to gemcitabine in patients with pancreatic cancer. *Clin Cancer Res*. 2011;17(17):5793–5800.
45. Evans PM, et al. Kruppel-like factor 4 is acetylated by p300 and regulates gene transcription via modulation of histone acetylation. *J Biol Chem*. 2007;282(47):33994–34002.
46. Rowland BD, et al. The KLF4 tumour suppressor is a transcriptional repressor of p53 that acts as a context-dependent oncogene. *Nat Cell Biol*. 2005;7(11):1074–1082.
47. Zhou Z, et al. New insight into the significance of KLF4 PARylation in genome stability, carcinogenesis, and therapy. *EMBO Mol Med*. 2020;12(12):e12391.
48. Zhang X, et al. SIRT1 deacetylates KLF4 to activate Claudin-5 transcription in ovarian cancer cells. *J Cell Biochem*. 2018;119(2):2418–2426.
49. Zhuo W, et al. Long noncoding RNA GMAN, up-regulated in gastric cancer tissues, is associated with metastasis in patients and promotes translation of Ephrin A1 by Competitively Binding GMAN-AS. *Gastroenterology*. 2019;156(3):676–691.
50. Mai D, et al. PIWI-interacting RNA-54265 is oncogenic and a potential therapeutic target in colorectal adenocarcinoma. *Theranostics*. 2018;8(19):5213–5230.
51. Li H, et al. A novel microRNA targeting HDAC5 regulates osteoblast differentiation in mice and contributes to primary osteoporosis in humans. *J Clin Invest*. 2009;119(12):3666–3677.
52. Wang X, et al. miR-214 targets ATF4 to inhibit bone formation. *Nat Med*. 2013;19(1):93–100.